Topological Arrangement of Cardiac Fibroblasts Regulates Cellular Plasticity

Jingyi Yu,[1,2,3,4,5,6], Marcus M Seldin [1,2,7], Kai Fu[3,4,5,6], Shen Li[1,2,3,4,5,6], Larry Lam[3,4,5,6], Ping Wang[1,2,3,4,5,6], Yijie Wang[1,2,3,4,5,6], Dian Huang[8], Thang L. Nguyen[8], Bowen Wei[9], Rajan P Kulkarni[6,9], Dino Di Carlo[6,8], Michael Teitell[5,6,10], Matteo Pellegrini[3,4,5,6], Aldons J Lusis[1,2,7] , Arjun Deb*[1,2,3,4,5,6]

[1]Division of Cardiology, Department of Medicine, University of California, Los Angeles, CA 90095; [2]Cardiovascular Research Laboratory, University of California, Los Angeles, CA 90095; [3]Department of Molecular, Cell and Developmental Biology, University of California, Los Angeles, CA 90095, U.S.A.; [4]Eli & Edythe Broad Center of Regenerative Medicine and Stem Cell Research, University of California, Los Angeles, CA 90095, U.S.A.; [5]Molecular Biology Institute, University of California, Los Angeles, CA 90095; [6]Jonsson Comprehensive Cancer Center, University of California, Los Angeles, CA 90095, U.S.A.; [7]Departments of Human Genetics & Microbiology, Immunology and Molecular Genetics, University of California, Los Angeles, CA 90095, U.S.A.; [8]Department of Bioengineering, University of California, Los Angeles, CA 90095; [9]Division of Dermatology, Department of Medicine, David Geffen School of Medicine, University of California, Los Angeles, CA 90095, U.S.A.; [10]Department of Pathology and Laboratory Medicine, David Geffen School of Medicine, University of California, Los Angeles, CA 90095, U.S.A.

J.Y., M.M.S., and K.F. contributed equally to this manuscript.

Running title: Topological States Regulate Fibroblast Plasticity

Subject Terms:
Heart Failure
Myocardial Infarction
Remodeling

Address correspondence to:
Dr. Arjun Deb
3609A MRL
675 Charles E Young Drive S.
University of California
Los Angeles, CA 90095
U.S.A.
Tel: 310-825-9911
adeb@mednet.ucla.edu.

In March 2018, the average time from submission to first decision for all original research papers submitted to *Circulation Research* was 10.69 days

ABSTRACT

Rationale: Cardiac fibroblasts do not form a syncytium but reside in the interstitium between myocytes. This topological relationship between fibroblasts and myocytes is maintained throughout post-natal life until acute myocardial injury occurs, when fibroblasts are recruited to, proliferate and aggregate in the region of myocyte necrosis. The accumulation or aggregation of fibroblasts in the area of injury thus represents a unique event in the life cycle of the fibroblast but little is known about how changes in the topological arrangement of fibroblasts following cardiac injury affect fibroblast function.

Objective: The objective of the study was to investigate how changes in topological states of cardiac fibroblasts (such as following cardiac injury) affect cellular phenotype.

Methods and Results: Using two and three-dimensional (2D vs 3D) culture conditions, we show that simple aggregation of cardiac fibroblasts is sufficient by itself to induce genome wide changes in gene expression and chromatin remodeling. Remarkably, gene expression changes are reversible following the transition from a 3D back to 2D state demonstrating a topological regulation of cellular plasticity. Genes induced by fibroblast aggregation are strongly associated and predictive of adverse cardiac outcomes and remodeling in mouse models of cardiac hypertrophy and failure. Using solvent based tissue clearing techniques to create optically transparent cardiac scar tissue, we show that fibroblasts in the region of dense scar tissue express markers that are induced by fibroblasts in the 3D conformation. Finally, using live cell interferometry, a quantitative phase microscopy technique to detect absolute changes in single cell biomass, we demonstrate that conditioned medium collected from fibroblasts in 3D conformation compared to that from a 2D state significantly increases cardiomyocyte cell hypertrophy.

Conclusions: Taken together, these findings demonstrate that simple topological changes in cardiac fibroblast organization are sufficient to induce chromatin remodeling and global changes in gene expression with potential functional consequences for the healing heart.

Keywords:
Remodeling, fibrosis, gene expression and regulation, cell biology, hypertrophy, fibroblasts, stem cell plasticity.

Nonstandard Abbreviations and Acronyms:

Acta2	alpha smooth muscle actin 2
ADAMTS15	metallopeptidase with thrombospondin motif 15
ATAC	assay for transposase accessible chromatin
Cnn2	Calponin 2
CTGF	connective tissue growth factor
EMT	epithelial-mesenchymal-transition
GO	Gene ontology
GPNMB	Glycoprotein non metastatic b
HMDP	Hybrid Mouse Diversity Panel
LCI	Live cell interferometry
MMP	Matrix Metalloproteinase
NRVM	Neonatal rat ventricular cardiomyocytes
PC	principle component
WGA	wheat germ agglutinin

INTRODUCTION

Cardiac fibroblasts develop from epithelial-mesenchymal-transition (EMT) of epicardial cells during cardiac development[1]. Following adoption of the mesenchymal phenotype, they migrate into the developing myocardium and as the myocardium compacts, they get trapped between the myocyte interstitium to become resident cardiac fibroblasts. This topological arrangement of fibroblasts and myocytes persists throughout post-natal life. However, this spatial relationship is disrupted following acute myocardial necrosis, when fibroblasts are recruited to, proliferate and aggregate in the region of injury, resulting in a much higher density of fibroblasts in the region of necrosis[2]. Aggregating fibroblasts in the region of injury are known to express gap junctions that facilitate intercellular communication between physically apposed fibroblasts[3]. Tumor cells and cancer cell lines, when cultured in 3D conditions to promote aggregation exhibit altered phenotypic features such as migration, proliferation and chemo resistance associated with changes in gene expression profiles[4]. However, little is known about how spatial rearrangement of fibroblasts such as that occurs after acute myocardial injury affects the cellular and genetic outputs of the fibroblast and the cardiac wound healing response.

METHODS

All data and supporting materials are within the article and online supplementary files. In addition, RNA-seq and ATAC-seq data for the study are available in NCBI's Gene Expression Omnibus and have been made publicly available through GEO series accession number GSE113277 at https://www.ncbi.nlm.nih.gov/geo/query/acc.cgi?acc=GSE113277.

Cardiac fibroblasts were isolated from adult wild type mice (both male and female) as well as Col1a2CreERT:R26R^{tdtomato} and TCF21MerCreMer:R26R^{tdtomato} as described[5]. Isolated cardiac fibroblasts (< 3 passages) were grown on standard polystyrene coated tissue culture plates (2D) (plates not coated with collagen or other matrix proteins) or seeded onto ultra-low attachment plates (not coated with any extracellular matrix protein), whereby they formed spheres within 24 hours of seeding (3D). Subsequently, the cardiac fibroblasts were again transferred back to regular tissue culture plates, on which the spheres attached and fibroblasts migrated out of the spheres to form monolayers within 4-5 days (3D-2D). Reseeding of the fibroblasts onto ultra-low attachment plates again resulted in formation of spheres within 24 hours (3D-2D-3D). Fibroblasts in 2D or 3D maintained for 5 days served as temporally adjusted controls for 3D-2D states. 3D-2D fibroblasts trypsinized and reseeded onto 2D states served as additional controls for 3D-2D-3D states. RNA-seq and ATAC-seq was performed at each topological state of the cardiac fibroblast and on temporally adjusted controls for each time point. Transcripts upregulated in 3D states were correlated to clinical traits across a mouse population (HMDP) following isoproterenol infusion[6]. Cardiac fibroblasts were also seeded onto tissue culture plates of varying stiffness (0.5kPa, 8kPa and 64kPa elastic moduli) to determine whether 2D-3D gene expression changes were recapitulated by modulating substrate stiffness. Optical transparency of the heart was performed with solvent based tissue clearing[7] and imaging performed with a Nikon C2+ confocal microscope. Immunofluorescent staining was performed using standard methods[5]. Conditioned medium was collected from 2D or 3D cardiac fibroblasts exactly 24 hours after initial seeding. LCI was performed to track changes in cell biomass of single neonatal rat ventricular cardiomyocytes with 2D or 3D conditioned medium.

RESULTS

To determine whether aggregation of cardiac fibroblasts affects the cellular phenotype, we first created a scaffold-free 3D system using ultra-low attachment tissue culture dishes where a covalently bonded hydrogel layer on the surface of the dish prevents cell attachment[8]. Cardiac fibroblasts were isolated from adult mice, and cells that had not undergone more than 3 passages were used for experiments. Seeding of primary adult mouse cardiac fibroblasts onto ultra-low attachment dishes resulted in fibroblasts aggregating together within 24 hours to form 3D spherical clusters (Fig 1A, B). To confirm that cardiac fibroblasts alone were capable of forming these spherical clusters, we next isolated cardiac fibroblasts from uninjured hearts of TCF21MerCreMer:R26R^{tdTomato} and Col1a2CreERT:R26R^{tdTomato} mice[5, 9, 10]. We and others have shown that the inducible Cre drivers are specific for genetic labeling of cardiac fibroblasts following tamoxifen administration. Similar to cardiac fibroblasts from wild type animals, genetically labeled cardiac fibroblasts within 24 hours of seeding onto ultra-low attachment plates also formed spherical clusters confirming the ability of cardiac fibroblasts to form 3D spherical aggregates under defined conditions (Fig 1C). Imaging Flow cytometry[11] demonstrated that aggregation into a 3D state resulted in significantly smaller small cell size (cell diameter: 22.45±0.30um in 2D versus 18.41±0.26; mean±S.E.M; $p<0.001$) and surface area (449.85±3.05um^2 in 3D versus 297.97±8 um^2; mean±S.E.M; $p<0.001$) (Fig 1D) suggestive of cellular remodeling as fibroblasts adopt the 3D state. To determine whether a switch from a 2D to a 3D state changes fibroblast phenotype, we first compared global gene expression changes by RNA-seq between cardiac fibroblasts cultured under standard 2D conditions on regular tissue culture dishes and 3D conditions as mentioned above (Fig 1A). For this purpose, cardiac fibroblasts were seeded onto standard tissue culture plates or ultra-low attachment plates with similar seeding density and identical cell culture medium and cells were harvested 24 hours later for gene expression analysis. To ask whether observed changes were reversible, we transferred 3D cardiac fibroblasts to regular tissue culture plates to put them back in 2D conditions (group termed 3D-2D) (Fig 1A). Spherical clusters of 3D fibroblasts attached to regular tissue culture plates and the fibroblasts migrated from spherical cluster to a monolayer within 4-5 days. We again determined gene expression of 3D-2D fibroblasts (following transition from 3D to a monolayer) to determine whether the gene expression pattern reverted to that of the 2D state (Fig 1A). Finally, cardiac fibroblasts which had been grown under 3D conditions and then transferred to 2D conditions (3D-2D) were put back under 3D conditions (group termed 3D-2D-3D). Sphere formation occurred within 24 hours of reseeding on ultra-low attachment plates and RNA-seq was performed to determine whether re-adoption of the 3D state was associated with gene expression signatures flipping back to the 3D state (Fig 1A). These experiments would thus determine whether changes in topological states or spatial arrangement of cardiac fibroblasts are associated with reversible and dynamic changes in gene expression. RNA-seq was performed for all the different topological states of the cardiac fibroblast and clustering of sample correlations demonstrated a grouping of all 2D fibroblast states, and a separate grouping of 3D fibroblast states (Fig 1E). The gene expression profile of 2D cardiac fibroblasts was like that of the 3D-2D fibroblast group while the gene expression profile of 3D fibroblasts was like that of the 3D-2D-3D group (Fig 1E). We observed a remarkable dynamic and reversible plasticity between the 2D and 3D states (Online Table I, Fig 1F, G). Out of 997 genes that were upregulated in 3D fibroblasts, expression of 996 genes reverted back when the 3D fibroblasts were transitioned back to the 2D state (3D-2D group) and re-induced following transition to 3D (3D-2D-3D group) (Fig 1F). Similarly, genes downregulated in 3D state exhibited increased expression following transition to the 2D state (3D-2D group) and silencing upon transitioning back to 3D (3D-2D-3D group) (Fig 1G). To adjust for potential temporal changes in gene expression, the gene expression pattern of the 3D-2D group was also compared to that of 2D and 3D fibroblasts cultured for 5 days. A cluster analysis demonstrated distinct clustering of 2D and 3D states (Online Fig IA). In addition, for the 3D-2D-3D group, temporally adjusted controls of 3D-2D cells lifted and reseeded back onto 2D instead of 3D conditions was also used **(Online Fig IB).** Again, cluster analysis demonstrated distinct 2D and 3D states making it unlikely that differential gene expression was simply secondary to temporal dependent changes in gene expression of cardiac fibroblasts in culture.

We next examined whether dynamic changes in gene expression in different topological states can be simply explained by sudden changes in substrate stiffness as the fibroblasts transition from a 2D adherent state to a 3D spherical non-adherent state. To answer this question, we seeded cardiac fibroblasts onto tissue culture plates coated with biocompatible silicone controlled elastic moduli recapitulating environments similar to tissue[12]. We seeded cardiac fibroblasts on tissue culture plates with stiffness of 0.8kpA, 8kPa and 64kPa (Online Fig IIA) and following 24 hours of seeding, harvested the cells to compare changes in gene expression to that of 2D and 3D topological states. Analysis of global gene expression demonstrated a clustering of 2D states with that of cells seeded at different substrate stiffness (0.5, 8, 64 kpA) and were distinct from gene expression signature of cardiac fibroblasts in 3D states (Online Fig IIB). We specifically examined the set of genes that displayed the highest degree of differential expression between 2D and 3D states and observed that the expression pattern of such genes was similar between cells seeded at 0.8,8 and 64kPA and 2Dstates and distinct from that seen in 3D states (Online Fig IIC, D). Taken together, these observations suggest that topological changes in cardiac fibroblasts drive gene expression patterns and changes in substrate stiffness are unlikely to underlie differences in gene expression between 2D and 3D states. We next examined the pool of genes that were the most upregulated (Fig 1F) or downregulated (Fig 1G) in 3D versus 2D fibroblast states. Gene ontology (GO) analysis demonstrated that genes downregulated in the 3D state mainly comprised cell cycle processes such as DNA replication, chromosomal condensation/segregation and cytokinesis (Fig 1H). Transcripts differentially upregulated in the 3D state involved pathways regulating extracellular matrix metabolism/proteolysis, surface proteins, chemotaxis and immune response. (Fig 1H, Online Table II). We next specifically examined several genes which were highly differentially expressed between 3D versus 2D fibroblasts and that are also known to regulate extracellular matrix such as metalloproteinases/metallopeptidases, [Metalloproteinase (MMP11, MMP2), ADAMTS15 (metallopeptidase with thrombospondin motif 15)], connective tissue growth factor (CTGF) and fibroblast contractility, alpha smooth muscle actin 2 (Acta2), Calponin (Cnn2) and modulators of inflammatory response (Glycoprotein non metastatic b, GPNMB). Based on RNA-seq patterns, expression of these genes was reversible and highly dependent upon the topological state of the fibroblast (Fig 2). For instance, MMP11 and MMP2 were highly induced following aggregation and sphere formation of fibroblasts but expressions declined to 2D levels when the 3D fibroblasts were allowed to attach and grow out as a monolayer for a few days (Fig 2A, B). However, reseeding the cells back to a 3D conformation led to rapid re-induction of MMP2/MMP11 expression illustrating the dynamic plasticity of the system (Fig 2A, B). Gene expression of Acta2, Cnn2, ADAMTS15, GPNMB and CTGF, which are thought to play a role in fibroblast contractility and regulation of inflammation and extracellular matrix, demonstrated similar patterns of changes of gene expression dependent upon the topological state (Fig 2C-G).

To determine whether such gene expression changes are associated with changes in phenotype, we first determined changes in cardiac fibroblast proliferation in the 3D versus 2D state. For this purpose, cardiac fibroblasts either in the 2D or 3D state were treated with EdU for 4 hours followed by determination of EdU uptake by flow cytometry. Consistent with decreased expression of cell cycle genes in the 3D state, we observed that 5.47±1.4% of cardiac fibroblasts in the 2D state were cycling (EdU uptake) versus 0.15±0.05% in the 3D state ($p<0.05$) (Fig 3A). Similarly, the fraction of cells expressing Ki67 (marker of proliferation) significantly decreased from 10.94±3.0% of cardiac fibroblasts in the 2D state to 1.0±0.08% in the 3D state ($p<0.05$) (Fig 3B). Western blotting with quantitative densitometry demonstrated that fibroblasts in the 3D state exhibit decreased expression of contractile proteins alpha smooth muscle actin (88±6% decrease in 3D versus 2D, $p<0.001$) and calponin (54±6% decrease in 3D versus 2D; $p<0.001$) (Fig 3C), consistent with gene expression data demonstrating decreased expression of myofibroblast proteins. Differentially expressed genes between the 2D and 3D states included genes affecting extracellular matrix catabolism. Collagen is the most common abundant extracellular matrix protein secreted by cardiac fibroblasts and we next determined how adoption of the 3D state affects collagen production. We measured total collagen using the Sircoll assay in 2D and 3D fibroblasts and observed that the total cellular collagen content significantly decreased from 8.40±2.8ug/10^6 cells in 3D states to 1.32±0.71/10^6 cells in 2D states

($p<0.05$) **(**Fig 3D). Cardiac fibroblasts secrete extracellular matrix proteins but are also known to express matrix degrading enzymes and can undergo de-differentiation as well[13]. These data suggest that a transition from a 2D to a 3D state leads to a switch of cardiac fibroblast phenotype from a matrix synthetic to a non-synthetic de-differentiated state. Recent evidence suggests that aggregation of cardiac fibroblasts in the area of myocardial injury is associated with fibroblasts exhibiting evidence of polarization[14]. Polarization or alignment of cardiac fibroblasts is thought to play a critical role in appropriate cardiac wound healing[15]. We thus examined whether 3D cardiac fibroblasts exhibited any evidence of polarization compared to 2D fibroblasts. To address this question, we examined expression of genes that are members of the *Frizzled (Fzd)*, *Van Gogh* (*Vangl* in vertebrates*)* and *Flamingo* (*Celsr* in vertebrates) (Fig 3E). These families of genes initially identified in drosophila are now known to play critical role in planar cell polarity and cellular orientation in epithelial and mesenchymal cells of vertebrates as well[16]. Within this subset of genes known to regulate cellular polarity, we observed that Frizzled 1 (Fzd1) expression was significantly higher in 3D compared to 2D states (Fig 3E). Fzd1 is a cell surface receptor and we performed flow cytometry to demonstrate that Fzd 1 expression was significantly up-regulated in 3D fibroblasts (Fig 3F) consistent with gene expression changes. Members of the frizzled family are known to be expressed in fibroblasts in the area of injury following myocardial injury and thought to contribute to cardiac remodeling and have been considered as therapeutic targets for augmenting cardiac repair[14, 17, 18]. In this regard, cardiac fibroblasts in 3D states recapitulate to a certain extent the expression of polarity genes known to be important for wound healing *in vivo*. Taken together, these observations demonstrate that aggregation and changes in spatial arrangement of cardiac fibroblasts can drive rapid, dynamic and reversible expression of genes affecting a panoply of processes regulating wound healing such as fibroblast proliferation, activation, collagen content and cell polarity.

We next investigated the mechanistic basis of such rapid and reversible changes in gene expression. We hypothesized that dynamic changes in chromatin structure may contribute at least in part to the rapid changes in gene expression seen following the transition of fibroblasts from a 2D to 3D state. Therefore, changes in chromatin organization and DNA accessibility (open and closed chromatin) were examined between cardiac fibroblasts in 2D versus 3D states by performing an assay for transposase accessible chromatin (ATAC-seq)[19]. ATAC-seq enables identification of open and closed regions of chromatin across the genome and provides insights about regions of the genome that are more (open) or less accessible (closed) to transcription factors[19]. We observed that there were significant changes in global chromatin organization (Fig 4A). Approximately 23% of the genes differentially upregulated in fibroblast 3D states and 18% of the genes downregulated in fibroblast 3D state (i.e. upregulated in 2D states) underwent significant changes in chromatin accessibility (Fig 4A) with remarkable concordance with their RNA-seq profiles. Both these values were significantly enriched over background levels as we observed that only 10% of all genes had differential ATAC-seq peaks upon transition from a 2D to 3D state (Fig 4A). We next examined differential ATAC-seq peaks for specific genes such as MMP2 and CTGF that demonstrated significant induction and silencing of gene expression respectively in the 3D state and observed significant differences in ATAC-seq peaks in their respective genomic loci, correlating with changes in gene expression (Fig 4B, C). These observations suggest that fibroblast aggregation and changes in spatial arrangement of cardiac fibroblasts are sufficient to induce changes in chromatin structure or organization that contributes to the global changes in genes expression between the 2D and 3D state.

Having demonstrated that changes in fibroblast aggregation and spatial arrangement are associated with concordant changes in the epigenome and gene expression, we next investigated the functional connotations of such global changes in gene expression for cardiac wound healing. Like humans, genetically diverse strains of mice differ in the degree of fibrosis or cardiac remodeling following pathological cardiac stressors and offer the advantage of tissue availability and experimental manipulation. The Hybrid Mouse Diversity Panel (HMDP) is a collection of genetically diverse mouse strains and allows sufficient power for genome wide association analysis to determine how genetic architecture impacts phenotypic traits [20-23]. A single pathologic stressor can be thus applied across all strains within the HMDP

to perform genome wide association studies and determine how genetic and environmental interactions contribute to global gene expression and clinical phenotypes[24]. In these studies, 96 strains of mice were administered a three-week continuous infusion of isoproterenol via osmotic pump[6]. Throughout the study, various physiological characteristics including cardiac functional indices (e.g. ejection fraction, left ventricular internal dimensions in end systole and diastole), metabolic parameters and tissue weights (61 traits in all) were measured (Online Table III) and the left ventricle of each mouse strain was subjected to global expression arrays[6, 24]. In this study, the mice responded dramatically to isoproterenol, as nearly every individual showed increased left ventricular mass following treatment. This dataset enabled us to assess whether differentially expressed genes between 3D and 2D states of cardiac fibroblasts could inform phenotypic traits known to predict outcomes or disease severity in isoproterenol induced cardiac hypertrophy and failure.

Initially we asked whether significantly upregulated transcripts in all 3D fibroblast states (compared to 2D) were correlated with heart failure traits in the HMDP. By simply correlating individual 3D up-regulated genes from our RNA-sequencing experiment across clinical traits in the mouse population (Online Fig III), we observed striking patterns of significance (Fig 5A). Since these patterns are difficult to interpret on a gene by-gene basis, we used a data reduction method to establish vectors which represent 3D specific gene signatures. Principle component (PC) approaches provide a means of data-reduction whereby variation across any number of dimensions can be aggregated into single or multiple vectors. Similar approaches utilizing a principle component to represent large gene sets are commonly utilized in population-based studies [6, 25]. These produce a series of vectors which represent a given pattern of variation, referred to as eigenvectors. Here, we applied this approach to gene expression, where the genes identified from the 2D vs 3D analysis were analyzed across a mouse population. We generated principle component (PC) eigengenes which captured 14.4% (PC1) and 6.8% (PC2) of the variation of all 3D-upregulated transcripts within the HMDP expression arrays (Fig 5B). It is worth mentioning that these values are fairly typical when performing principle component analysis on population-wide data (here, we use ~600 genes within ~100 strains of mice), especially given the significant variation observed in gene expression profiles. Using these eigengenes (PC1 & PC2) as signatures of 3D fibroblast genes, we plotted the position of each strain against various cardiac and non-cardiac clinical traits. Cardiac fibroblasts are known to affect cardiac hypertrophy and play a major role in adverse cardiac remodeling and dilatation of the cardiac chambers, clinically determined by the left ventricular dimensions in end systole and diastole. Consistent with this notion, we observed highly significant positive correlations between 3D fibroblast derived gene signatures and left ventricular dimensions in both end diastole (Fig 5C, D) and end systole (Fig 5E, F) as well as cardiac mass (Fig 5G, H). Notably these 3D fibroblast eigengene signatures did not correlate with either heart rate (Fig 5I, J) or non-cardiac traits such as plasma glucose (Fig 5K, L) demonstrating specificity of these eigengene signatures to cardiac remodeling traits. Collectively, these data show that 3D fibroblast enriched transcripts show striking patterns of correlation with adverse cardiac indices such as cardiac hypertrophy and chamber dilatation across the murine population following isoproterenol infusion.

So far, our data demonstrates that cardiac fibroblasts exhibit a high degree of dynamic plasticity with induction and silencing of genes following transition from a 2D to 3D state. Genes induced in the 3D state significantly correlated with clinical indices of adverse ventricular remodeling. Therefore, we next determined whether genes differentially expressed in the 3D state were also upregulated in regions of fibroblast aggregation in vivo at the time of wound healing. For this purpose, we performed cryo-injury on hearts of Col1a2CreERT:R26R^{tdtomato} and TCF21MerCreMer:R26R^{tdtomato} mice following tamoxifen mediated labeling of cardiac fibroblasts. Tamoxifen was administered for 10 days to label the cardiac fibroblasts and stopped 5 days prior to cryo-injury. We chose cryo-injury as cryo-injury unlike ischemic myocardial injury creates a highly well-defined compact transmural scar on the left ventricle and the tdTomato labeling of cardiac fibroblasts can easily identify regions of compact scarring. Hearts were harvested at 7 days following cryo-injury and immunofluorescent staining performed to determine whether

genes highly upregulated in 3D fibroblasts *in vitro* were expressed by labeled cardiac fibroblasts or expressed in abundance in the region of fibroblast aggregation. We observed abundant expression of MMP11 by tdTomato labeled cardiac fibroblasts but minimal MMP11 expression in uninjured regions (Fig 6A-D). ADAMTS15, a secreted protein that regulates extracellular matrix, is expressed in the developing heart and highly induced in the 3D fibroblast state (Supplementary Table 1), was also found to be abundantly present in the injured region and expressed by tdTomato labeled fibroblasts (Fig 6E-H). To study the expression of 3D enriched transcripts in aggregating fibroblasts in regions of injury in greater detail, we subjected the harvested heart to solvent based tissue clearing techniques to make the heart optically transparent[7]. This allows the entire 3D structure of the scar to be visualized in detail without having to extrapolate and reconstruct a 3D structure from conventional analysis of histological sections. We again performed cryo-injury on Col1a2CreERT:R26R^{tdtomato} mice following fibroblast labeling. We harvested the heart 7 days after cryo-injury and made them optically transparent and a non-absorbable suture (placed at the time of injury) was used to identify area of cryo injury in the heart after tissue clearing (Fig 6I-K). The region of injury could be identified easily as an area with accumulation of tdTomato labeled cardiac fibroblasts (Fig 6L). On the optically cleared heart, we performed immunostaining for another marker GPNMB, a gene upregulated in the 3D state, involved with immune response pathways and that strongly correlated with adverse cardiac remodeling indices in our murine model of isoproterenol induced heart failure. Analysis of Z stacked confocal images taken sequentially through the whole depth of the scar demonstrated expression of GPNMB by tdTomato labeled fibroblasts throughout the depth of the scar (Fig 6M). These observations demonstrate that genes expressed by aggregating fibroblasts in the region of injury at least partially recapitulate the gene expression signatures of 3D fibroblasts.

Fibroblasts are known to affect cardiac hypertrophy[26] and the gene expression signatures of 3D fibroblasts strongly correlated with clinical indices of heart mass and remodeling across mouse strains. We next investigated whether fibroblasts in 3D exert pro-hypertrophic effects on cardiomyocytes compared to fibroblasts cultured in 2D. For this purpose, we collected conditioned medium from fibroblasts grown in 3D or 2D conditions for 24 hours. We treated neonatal rat cardiomyocytes with 3D or 2D conditioned medium to determine effects on cardiomyocyte hypertrophy over the next 48 hours. Live cell interferometry (LCI), a validated version of quantitative phase microscopy [27, 28] is an extremely sensitive tool for determining changes in total cellular biomass. LCI is based on the principle that light slows as it interacts with matter. As light traverses through a cell that has greater biomass (i.e. hypertrophied), the light slows and its waveform shifts in phase compared to light not passing through the cell [29](Fig 6N). The change in phase shift over time is directly related to the change in biomass of the cell over time and this quantitative phase shift has been used to precisely and reproducibly determine the dry biomass of cells including T cells, stem cells, cancer cells and fibroblasts [27, 28]. Neonatal rat ventricular cardiomyocytes (NRVM) were treated with conditioned medium as above and each cardiomyocyte was subjected to repeated measurements by LCI to obtain a growth rate. We observed that 2D conditioned medium significantly increased the rate of cardiomyocyte biomass accumulation compared to non-conditioned medium (0.4 picogram/hr for 2D compared to -0.12 picogram/hour for growth medium, p=0.04) (Fig 6O). However, treatment with 3D conditioned medium tripled the rate of growth versus treatment with 2D conditioned medium (1.25 pg/hr for 3D versus 0.4 pg/hr for 2D, p=0.0001) (Fig 6O). As cardiomyocytes after isolation can exhibit significant difference in cell size, we normalized the growth rate of each cardiomyocyte to initial cell biomass. Again, we observed a significant 34% increase in cell biomass of NRVM following treatment with 2D conditioned medium compared to 'non-conditioned' growth medium (0.34% for 2D vs -0.01% for growth medium, p=0.02) (Fig 6P). However, 3D fibroblast conditioned medium significantly increased the cell biomass accumulation rate of NRVM by a further 88% compared to NRVM treated with 2D conditioned medium (0.64% for 3D versus 0.34% for 2D, p=0.002) (Fig 6P). These observations demonstrate that the secretome of fibroblasts in 3D is sufficient to induce cardiomyocyte hypertrophy and are broadly consistent with the genome-wide association data shown earlier demonstrating high correlation between genes induced in the 3D state and indices of cardiac hypertrophy and remodeling after

isoproterenol infusion. Our observations also suggest that the gene expression signatures adopted by aggregating fibroblasts may have a direct causal effect on a hypertrophic response after cardiac injury.

We next analyzed our RNA-seq data to obtain insight into transcription factors or transcriptional regulators that could be contributing to changes in gene expression between the 2D and 3D states and affecting myocyte hypertrophy. Genes differentially upregulated in the 3D versus 2D state were assayed for enrichment of upstream transcriptional factors or regulators using TRRUSTv2[30]. This analysis queries hundreds of published Chip-Seq and/or open chromatin data to infer regulatory elements from gene expression patterns. The 3D upregulated genes were used to identify enrichment of regulation by specific transcription factors or DNA binding elements known to regulate expression. We observed significant representation of several transcription factors predicted to regulate 3D-specific genes (Online Figure IV) and some of these are also known to regulate or be associated with the cardiac hypertrophic response such as Microphthalmia associated transcription factor (MITF), Beta catenin (CTNNB1) and serum response factor (SRF)[31-33]. Next, to obtain insight into secreted factors present in 3D conditioned medium that induced or contributed to myocyte hypertrophy, we filtered the differentially upregulated genes in the 3D state for secreted factors and observed expression of proteins known to affect the myocyte hypertrophic response such as angiotensinogen, pyrophosphatases affecting purinergic signaling (ENPP3) and members of the Wnt signaling family (Dkk3) (Online Table IV)[34-36].

DISCUSSION

Cardiac fibroblasts are known to be highly plastic and our study suggests that simple aggregation of fibroblasts may be sufficient to induce genome wide changes in chromatin reorganization and gene expression. We show that gene expression signatures adopted by aggregating cardiac fibroblasts at least in part recapitulates changes in gene expression in the injured region *in vivo* and that such altered genetic outputs may have functional consequences for cardiac wound healing and remodeling. Cardiac fibroblasts are the principal contributors towards deposition of extracellular matrix but are also known to secrete metalloproteinases and extracellular proteases that leads to degradation of extracellular matrix[37]. Acute myocardial injury is associated with significant upregulation in metalloproteinase activity[38] and MMP expression significantly increased in 3D cardiac fibroblasts mirroring such *in vivo* changes. A balance between the synthetic and proteolytic phenotype of the fibroblasts determines extracellular matrix content or burden of scar tissue in pathologic states. Augmented matrix synthetic and matrix degrading properties of cardiac fibroblasts can lead to high turnover of extracellular matrix, as seen in heart failure. Such fibroblast phenotypes with opposing effects on matrix synthesis and degradation, as seen in our 2D and 3D model could determine the burden of scar after acute and chronic injury and serve as a model for obtaining further mechanistic insight [39]. Although little is known about signaling mechanisms that regulate resolution of fibrosis, de-differentiation of contractile elements of fibroblasts with decreased expression of alpha smooth muscle actin is thought to represent a key event for fibrosis resolution[40]. In this regard, our model of fibroblast aggregation with decreased expression of smooth muscle actin and induction of various matrix degrading enzymes demonstrates phenotypic features consistent with myofibroblast de-differentiation and a proteolytic rather than a synthetic phenotype. The expression of alpha smooth muscle actin and other contractile proteins in fibroblasts in the injury region allows for wound contraction *in vivo*, a mechanism that enables reduction in the area of injury. Conversely, impaired expression of fibroblast contractile proteins or defects in fibroblast polarization in vivo can cause impaired wound contraction, dysregulated wound healing and lead to expansion of the infarcted region, a dreaded complication after myocardial infarction. Our model that demonstrates a rapid and reversible expression of contractile proteins in fibroblasts could serve as a platform for investigating the molecular events that abruptly can switch a cardiac fibroblast from a synthetic and contractile phenotype to a proteolytic and de-differentiated phenotype. Hypertrophy of surviving cardiac myocytes at the edges of the injured region occurs after myocardial

infarction and the 3D fibroblasts can serve as a platform for interrogating the paracrine effects of cardiac fibroblasts on myocyte hypertrophy. Given the global changes in gene expression and substantial changes in the 3D cardiac fibroblast secretome, it is likely that rather than a single driver, activity of multiple transcription factors and secreted proteins synergistically affect gene expression changes and the myocyte hypertrophic response.

Study of cells in spheroids have been performed for cancer cells and cells with progenitor potential. Our study suggests that studying fibroblasts in a 3D state in contrast to conventional analysis of 2D fibroblasts may be more informative of cellular changes in the injury region *in vivo*. Potentially, our model could also be used as a tool or a primary screening system to determine how drugs or small molecules affect changes in expression of specific genes that are upregulated in the 3D state or affect phenotypic transitions between matrix synthetic (2D) and matrix degrading (3D) states of a cardiac fibroblast.

ACKNOWLEDGEMENTS
We thank the UCLA Heart lab cell core for providing freshly isolated cardiomyocytes and the UCLA Clinical Microarray Core for RNA-sequencing. Imaging flow cytometry was performed in the UCLA Jonsson Comprehensive Cancer Center and Center for AIDS Research Flow Cytometry Core Facility. We thank Dr. Eric Olson, University of Texas Southwestern Medical Center and Dr. Andrew Leask, University of Western Ontario Canada for sharing the TCF21MerCreMer and Col1a2CreERT mice.

SOURCES OF FUNDING
The project was supported by grants from the NIH (HL129178, HL137241 to AD, CA185189, GM073981, GM114188 to MT, HL30568 and HL123295 to AJL, Department of Defense (PR152219, PR161247 to AD), Air Force Office of Scientific Research (FA9550-15-1-0406 to MT), California Institute of Regenerative Medicine (DISC1-08790 to AD), research award from the Eli and Edythe Broad Center of Regenerative Medicine and Stem Cell Research & Rose Hills Foundation to AD and planning award from the Eli and Edythe Broad Center of Regenerative Medicine and Stem Cell Research and California Nanosystems Institute at UCLA to AD and DC. The project also received support from NIH/NCATS UCLA CTSI (ULTR00024). Imaging flow cytometry at the UCLA Jonsson Comprehensive Cancer Center is supported by NIH awards P30 CA016042 and 5P30 AI028697.

DISCLOSURES
None.

REFERENCES

1. Manner J, Perez-Pomares JM, Macias D and Munoz-Chapuli R. The origin, formation and developmental significance of the epicardium: a review. *Cells Tissues Organs*. 2001;169:89-103.
2. Christia P, Bujak M, Gonzalez-Quesada C, Chen W, Dobaczewski M, Reddy A and Frangogiannis NG. Systematic characterization of myocardial inflammation, repair, and remodeling in a mouse model of reperfused myocardial infarction. *J Histochem Cytochem*. 2013;61:555-70.
3. Camelliti P, Borg TK and Kohl P. Structural and functional characterisation of cardiac fibroblasts. *Cardiovasc Res*. 2005;65:40-51.
4. Shoval H, Karsch-Bluman A, Brill-Karniely Y, Stern T, Zamir G, Hubert A and Benny O. Tumor cells and their crosstalk with endothelial cells in 3D spheroids. *Scientific Reports*. 2017;7:10428.
5. Pillai IC, Li S, Romay M, Lam L, Lu Y, Huang J, Dillard N, Zemanova M, Rubbi L, Wang Y, Lee J, Xia M, Liang O, Xie YH, Pellegrini M, Lusis AJ and Deb A. Cardiac Fibroblasts Adopt Osteogenic Fates and Can Be Targeted to Attenuate Pathological Heart Calcification. *Cell stem cell*. 2017;20:218-232 e5.
6. Rau CD, Romay MC, Tuteryan M, Wang JJ, Santolini M, Ren S, Karma A, Weiss JN, Wang Y and Lusis AJ. Systems Genetics Approach Identifies Gene Pathways and Adamts2 as Drivers of Isoproterenol-Induced Cardiac Hypertrophy and Cardiomyopathy in Mice. *Cell Syst*. 2017;4:121-128 e4.
7. Sung K, Ding Y, Ma J, Chen H, Huang V, Cheng M, Yang CF, Kim JT, Eguchi D, Di Carlo D, Hsiai TK, Nakano A and Kulkarni RP. Simplified three-dimensional tissue clearing and incorporation of colorimetric phenotyping. *Sci Rep*. 2016;6:30736.
8. Wang YJ, Bailey JM, Rovira M and Leach SD. Sphere-forming assays for assessment of benign and malignant pancreatic stem cells. *Methods Mol Biol*. 2013;980:281-90.
9. Ubil E, Duan J, Pillai IC, Rosa-Garrido M, Wu Y, Bargiacchi F, Lu Y, Stanbouly S, Huang J, Rojas M, Vondriska TM, Stefani E and Deb A. Mesenchymal-endothelial transition contributes to cardiac neovascularization. *Nature*. 2014;514:585-90.
10. Kanisicak O, Khalil H, Ivey MJ, Karch J, Maliken BD, Correll RN, Brody MJ, SC JL, Aronow BJ, Tallquist MD and Molkentin JD. Genetic lineage tracing defines myofibroblast origin and function in the injured heart. *Nat Commun*. 2016;7:12260.
11. Basiji D and O'Gorman MR. Imaging flow cytometry. *J Immunol Methods*. 2015;423:1-2.
12. Gutierrez E and Groisman A. Measurements of elastic moduli of silicone gel substrates with a microfluidic device. *PLoS One*. 2011;6:e25534.
13. Baudino TA, Carver W, Giles W and Borg TK. Cardiac fibroblasts: friend or foe? *Am J Physiol Heart Circ Physiol*. 2006;291:H1015-26.
14. Blankesteijn WM, Essers-Janssen YP, Verluyten MJ, Daemen MJ and Smits JF. A homologue of Drosophila tissue polarity gene frizzled is expressed in migrating myofibroblasts in the infarcted rat heart. *Nat Med*. 1997;3:541-4.
15. Kong P, Shinde AV, Su Y, Russo I, Chen B, Saxena A, Conway SJ, Graff JM and Frangogiannis NG. Opposing Actions of Fibroblast and Cardiomyocyte Smad3 Signaling in the Infarcted Myocardium. *Circulation*. 2018;137:707-724.
16. Yang Y and Mlodzik M. Wnt-Frizzled/planar cell polarity signaling: cellular orientation by facing the wind (Wnt). *Annu Rev Cell Dev Biol*. 2015;31:623-46.
17. Laeremans H, Hackeng TM, van Zandvoort MA, Thijssen VL, Janssen BJ, Ottenheijm HC, Smits JF and Blankesteijn WM. Blocking of frizzled signaling with a homologous peptide fragment of wnt3a/wnt5a reduces infarct expansion and prevents the development of heart failure after myocardial infarction. *Circulation*. 2011;124:1626-35.
18. Daskalopoulos EP, Hermans KC, Janssen BJ and Matthijs Blankesteijn W. Targeting the Wnt/frizzled signaling pathway after myocardial infarction: a new tool in the therapeutic toolbox? *Trends Cardiovasc Med*. 2013;23:121-7.
19. Buenrostro JD, Giresi PG, Zaba LC, Chang HY and Greenleaf WJ. Transposition of native chromatin for fast and sensitive epigenomic profiling of open chromatin, DNA-binding proteins and nucleosome position. *Nature methods*. 2013;10:1213-8.

20. Ghazalpour A, Rau CD, Farber CR, Bennett BJ, Orozco LD, van Nas A, Pan C, Allayee H, Beaven SW, Civelek M, Davis RC, Drake TA, Friedman RA, Furlotte N, Hui ST, Jentsch JD, Kostem E, Kang HM, Kang EY, Joo JW, Korshunov VA, Laughlin RE, Martin LJ, Ohmen JD, Parks BW, Pellegrini M, Reue K, Smith DJ, Tetradis S, Wang J, Wang Y, Weiss JN, Kirchgessner T, Gargalovic PS, Eskin E, Lusis AJ and LeBoeuf RC. Hybrid mouse diversity panel: a panel of inbred mouse strains suitable for analysis of complex genetic traits. *Mamm Genome*. 2012;23:680-92.
21. Lusis AJ, Seldin MM, Allayee H, Bennett BJ, Civelek M, Davis RC, Eskin E, Farber CR, Hui S, Mehrabian M, Norheim F, Pan C, Parks B, Rau CD, Smith DJ, Vallim T, Wang Y and Wang J. The Hybrid Mouse Diversity Panel: a resource for systems genetics analyses of metabolic and cardiovascular traits. *J Lipid Res*. 2016;57:925-42.
22. Bennett BJ, Farber CR, Orozco L, Kang HM, Ghazalpour A, Siemers N, Neubauer M, Neuhaus I, Yordanova R, Guan B, Truong A, Yang WP, He A, Kayne P, Gargalovic P, Kirchgessner T, Pan C, Castellani LW, Kostem E, Furlotte N, Drake TA, Eskin E and Lusis AJ. A high-resolution association mapping panel for the dissection of complex traits in mice. *Genome research*. 2010;20:281-90.
23. Patterson M, Barske L, Van Handel B, Rau CD, Gan P, Sharma A, Parikh S, Denholtz M, Huang Y, Yamaguchi Y, Shen H, Allayee H, Crump JG, Force TI, Lien CL, Makita T, Lusis AJ, Kumar SR and Sucov HM. Frequency of mononuclear diploid cardiomyocytes underlies natural variation in heart regeneration. *Nature genetics*. 2017;49:1346-1353.
24. Wang JJ, Rau C, Avetisyan R, Ren S, Romay MC, Stolin G, Gong KW, Wang Y and Lusis AJ. Genetic Dissection of Cardiac Remodeling in an Isoproterenol-Induced Heart Failure Mouse Model. *PLoS genetics*. 2016;12:e1006038.
25. Langfelder P and Horvath S. Eigengene networks for studying the relationships between co-expression modules. *BMC Syst Biol*. 2007;1:54.
26. Fujiu K and Nagai R. Fibroblast-mediated pathways in cardiac hypertrophy. *J Mol Cell Cardiol*. 2014;70:64-73.
27. Zangle TA, Burnes D, Mathis C, Witte ON and Teitell MA. Quantifying biomass changes of single CD8+ T cells during antigen specific cytotoxicity. *PLoS One*. 2013;8:e68916.
28. Zangle TA, Chun J, Zhang J, Reed J and Teitell MA. Quantification of biomass and cell motion in human pluripotent stem cell colonies. *Biophys J*. 2013;105:593-601.
29. Bon P, Maucort G, Wattellier B and Monneret S. Quadriwave lateral shearing interferometry for quantitative phase microscopy of living cells. *Opt Express*. 2009;17:13080-94.
30. Han H, Cho JW, Lee S, Yun A, Kim H, Bae D, Yang S, Kim CY, Lee M, Kim E, Lee S, Kang B, Jeong D, Kim Y, Jeon HN, Jung H, Nam S, Chung M, Kim JH and Lee I. TRRUST v2: an expanded reference database of human and mouse transcriptional regulatory interactions. *Nucleic acids research*. 2018;46:D380-D386.
31. Tshori S, Gilon D, Beeri R, Nechushtan H, Kaluzhny D, Pikarsky E and Razin E. Transcription factor MITF regulates cardiac growth and hypertrophy. *J Clin Invest*. 2006;116:2673-2681.
32. Bergmann MW. WNT signaling in adult cardiac hypertrophy and remodeling: lessons learned from cardiac development. *Circ Res*. 2010;107:1198-208.
33. Madonna R, Geng YJ, Bolli R, Rokosh G, Ferdinandy P, Patterson C and De Caterina R. Co-activation of nuclear factor-kappaB and myocardin/serum response factor conveys the hypertrophy signal of high insulin levels in cardiac myoblasts. *J Biol Chem*. 2014;289:19585-98.
34. Burnstock G. Purinergic Signaling in the Cardiovascular System. *Circ Res*. 2017;120:207-228.
35. Wang AY, Chan JC, Wang M, Poon E, Lui SF, Li PK and Sanderson J. Cardiac hypertrophy and remodeling in relation to ACE and angiotensinogen genes genotypes in Chinese dialysis patients. *Kidney international*. 2003;63:1899-907.
36. Foulquier S, Daskalopoulos EP, Lluri G, Hermans KCM, Deb A and Blankesteijn WM. WNT Signaling in Cardiac and Vascular Disease. *Pharmacol Rev*. 2018;70:68-141.
37. Travers JG, Kamal FA, Robbins J, Yutzey KE and Blaxall BC. Cardiac Fibrosis: The Fibroblast Awakens. *Circ Res*. 2016;118:1021-40.

38. DeLeon-Pennell KY, Meschiari CA, Jung M and Lindsey ML. Matrix Metalloproteinases in Myocardial Infarction and Heart Failure. *Prog Mol Biol Transl Sci*. 2017;147:75-100.
39. Fan D, Takawale A, Lee J and Kassiri Z. Cardiac fibroblasts, fibrosis and extracellular matrix remodeling in heart disease. *Fibrogenesis Tissue Repair*. 2012;5:15.
40. Jun JI and Lau LF. Resolution of organ fibrosis. *J Clin Invest*. 2018;128:97-107.

FIGURE LEGENDS

Figure 1. Cardiac fibroblasts exhibit dynamic changes in gene expression in different topological states. (A) Schematic of how fibroblasts were transitioned from a 2D to 3D state and then back to 2D and 3D respectively. For each topological state, fibroblasts were harvested for RNA-seq. **(B)** Bright phase image of cardiac fibroblasts in 2D and 3D (Scale bar: 50μm) **(C)** Pure population of genetically labeled (tdTomato) fibroblasts isolated by flow cytometry from hearts of TCF21MerCreMer:R26R^{tdtomato} or Col1a2CreERT:R26R^{tdtomato} mice were subjected to sphere formation (3D) and spheres stained with wheat germ agglutinin (WGA), that stains cell membranes (Scale bar: 20μm). **(D)** Cardiac fibroblasts in 2D or 3D states dissociated and subjected to image flow cytometry showing representative image of fibroblast from 2D or 3D state (3000 cells imaged in each group, scale bar:10μm) and corresponding mean diameter and surface area of fibroblasts in 2D or 3D states (*p<0.001, mean ± S.E.M., n=3) **(E)** Heat map demonstrating clustering of sample correlations of fibroblasts (shown by Z scores) in different topological states **(F,G)** Heat map comparing **(F)** expression of the most upregulated 3D genes in different topological states and **(G)** 3D downregulated genes in different topological states **(H)** GO analysis showing cellular pathways most affected by genes upregulated or downregulated in 2D/3D states.

Figure 2. Dynamic changes in expression of myofibroblast and extracellular matrix genes between 2D and 3D cardiac fibroblast states. (A, B) normalized gene counts on RNA-seq demonstrating rapid changes in gene expression of **(A)** MMP11 (B) MMP2, **(C)** Acta2 **(D)** Calponin **(E)** Connective tissue growth factor (CTGF) **(F)** ADAMTS15 and **(G)** GPNMB in cardiac fibroblasts in different topological states.

Figure 3. Changes in fibroblast phenotype in 3D versus 2D topological state. (A, B) Flow cytometry to determine fraction of proliferating fibroblasts in 2D and 3D states by **(A)** EdU uptake (5.48±1.4% in 2D versus 0.15±0.05% in 3D, mean ± S.E.M, p<0.05, n=3) or **(B)** Ki67 expression (10.14±3.0% in 2D versus 1.02±0.01% in 3D, mean ± S.E.M, p<0.05, n=3). **(C)** Western blotting and quantitative densitometry of expression of Alpha smooth muscle actin and calponin expression by cardiac fibroblasts in 2D or 3D states (mean ± S.E.M, *p<0.001, n=3). **(D)** Estimation of total collagen content of cardiac fibroblasts in 2D or 3D state (8.40±2.8μg/106 cells in 3D versus 1.32±0.71/106 cells in 2D, mean ± S.E.M, *p<0.05, n=3). **(E)** Heat map demonstrating expression of members of the Frizzled, Vangl and Celsr family in different topological states of cardiac fibroblasts. **(F)** Flow cytometry demonstrating Fzd1 expression in 3D versus 2D cardiac fibroblasts (2.07±0.33% in 2D versus 5.63±0.24% in 3D, mean ± S.E.M, p<0.05, n=3).

Figure 4. Chromatin changes underlie altered gene expression of fibroblasts in 3D versus 2D states. (A) ATAC seq performed to demonstrate fraction of genes demonstrating differential ATAC-seq peaks in either 2D or 3D cardiac fibroblast states **(B, C)** ATAC-seq peaks and RNA-seq showing expression of **(B)** MMP2 and **(C)** CTGF in 2D and 3D states demonstrating differential ATAC-seq peaks in loci of MMP2 and CTGF genes (numbers listed refer to scales of enrichment).

Figure 5. Genes enriched in 3D fibroblast states show significant correlation with indices of adverse ventricular modeling in HMDP studies following isoproterenol infusion. (A) Correlation heat map (yellow: positive and blue: negative correlation) of top 15 differentially upregulated genes in 3D/2D states versus clinical traits of left ventricular dimensions, heart mass, plasma glucose and heart rate following infusion of isoproterenol **(B)** Individual gene contribution to eigengene signatures PC1 and PC2 using transcripts enriched in 3D states. **(C-H)** Correlation of both eigengene signatures against cardiac and non-cardiac traits with significant correlation between both eigengenes and **(C, D)** LVID at end diastole **(E, F)** LVID at end systole and **(G, H)** total heart mass with no significant correlation between either eigengene and **(I-J)** heart rate and **(K, L)** plasma glucose (LVID: left ventricular internal diameter; bicor: bicorrelation coefficient).

Figure 6. Genes enriched in 3D fibroblasts are expressed in vivo in regions of fibroblast aggregation after heart injury and affect cardiomyocyte hypertrophy. (A-D) Immunofluorescent staining for MMP11 on uninjured and cryo-injured hearts of **(A, B)** TCF21MerCreMer:R26R^{tdtomato} and **(C, D)** Col1a2CreERT:R26R^{tdtomato} mice **(B, D)** area of injury shown in higher magnification demonstrating tdTomato labeled fibroblasts expressing MMP11 (arrows). **(E-H)** Immunofluorescent staining for ADAMTS15 on uninjured and cryo-injured hearts of **(E, F)** TCF21MerCreMer:R26R^{tdtomato} and **(G, H)** area of injury shown in higher magnification demonstrating tdTomato labeled fibroblasts expressing ADAMTS15 (arrows) (Scale bars: 20μm). **(I, J)** Cryo-injured heart of Col1a2CreERT:R26R^{tdtomato} mouse **(I)** prior to and **(J)** following optical clearing (arrowhead points to suture for identifying injured region, arrow points to green dye to identify area adjacent to injury; note the wire mesh on which the heart lies is now visible through the transparent heart; red arrow) **(K)** tdTomato fluorescence observed on cryo-injured Col1a2CreERT:R26R^{tdtomato} heart and **(L)** confocal image through area of injury showing intense tdTomato fluorescence (Scale bar: 500μm) **(M)** Immunofluorescent staining for GPNMB on optically cleared Col1a2CreERT:R26R^{tdtomato} heart after injury. The entire depth of the scar was imaged with a confocal microscope and sequential Z stack images demonstrating distribution of tdTomato (red), GPNMB (green) and merged (yellow) image demonstrating distribution of fluorophores across the depth of the scar (asterisk corresponds to position of suture). **(N)** Set up of live cell interferometry with phase shift of light being a read out for changes in cell biomass **(O)** Absolute and **(P)** normalized single cell cardiomyocyte (NRVM) biomass accumulation rates determined by serial measurements with interference microscopy over 48 hours following treatment of NRVM with growth medium (non-conditioned) or conditioned medium from fibroblasts in 2D or 3D state (each circle represents a single cardiomyocyte; Number of single cardiomyocytes tracked: 103 for growth medium, 142 for 2D medium and 231 for 3D medium).

Novelty and Significance

What Is Known?

- Unlike cardiac myocytes, cardiac fibroblasts do not form a syncytium but reside in the interstitium among myocytes.
- This topological relationship is altered after heart injury when fibroblasts are recruited to and aggregate at the area of injury.
- Aggregation of fibroblasts after injury thus represents a unique event in the life cycle of the cardiac fibroblast but whether such topological rearrangement affects fibroblast function is not clear

What New Information Does This Article Contribute?

- Aggregation of cardiac fibroblasts leads to global changes in gene expression and chromatin reorganization.
- Changes in the transcriptome are reversible upon aggregation, disaggregation and reaggregation of cardiac fibroblasts.
- Genes induced by fibroblast aggregation are expressed in the injured heart and correlate with poor cardiac outcomes in mouse models of hypertrophy and heart failure.
- The secretome of aggregated cardiac fibroblasts can induce hypertrophy of cardiac myocytes.

Cardiac fibroblasts reside in the interstitium of the heart and do not form a syncytium. Following injury, they however are recruited to aggregate in the area of injury, but the physiological significance of fibroblast aggregation remains unknown. Here, we demonstrate that simple aggregation of cardiac fibroblasts induces wide spread changes in gene expression and chromatic reorganization. Such transcriptional changes are reversible when cardiac fibroblasts are disaggregated or subsequently reaggregated. Genes upregulated in the aggregated state are expressed in the region of injury and correlate with indices of adverse cardiac remodeling in murine models of cardiac hypertrophy and failure. Finally, we demonstrate that the secretome of aggregated cardiac fibroblasts induces hypertrophy of cardiac myocytes. Taken together these observations demonstrate that topological changes in the spatial organization of cardiac fibroblasts drives chromatin reorganization, gene expression patterns and has functional consequences for cardiac wound healing.

FIGURE 1

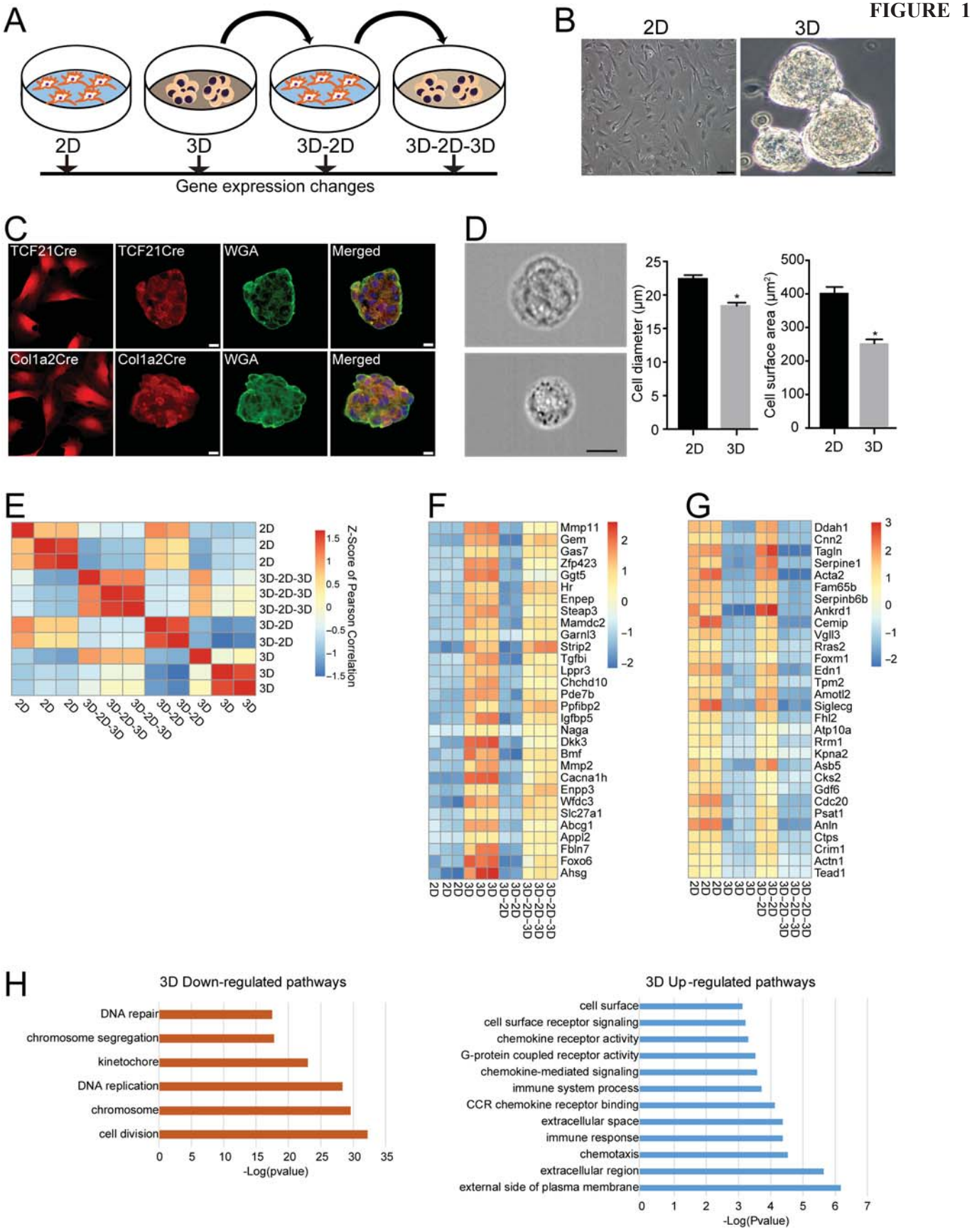

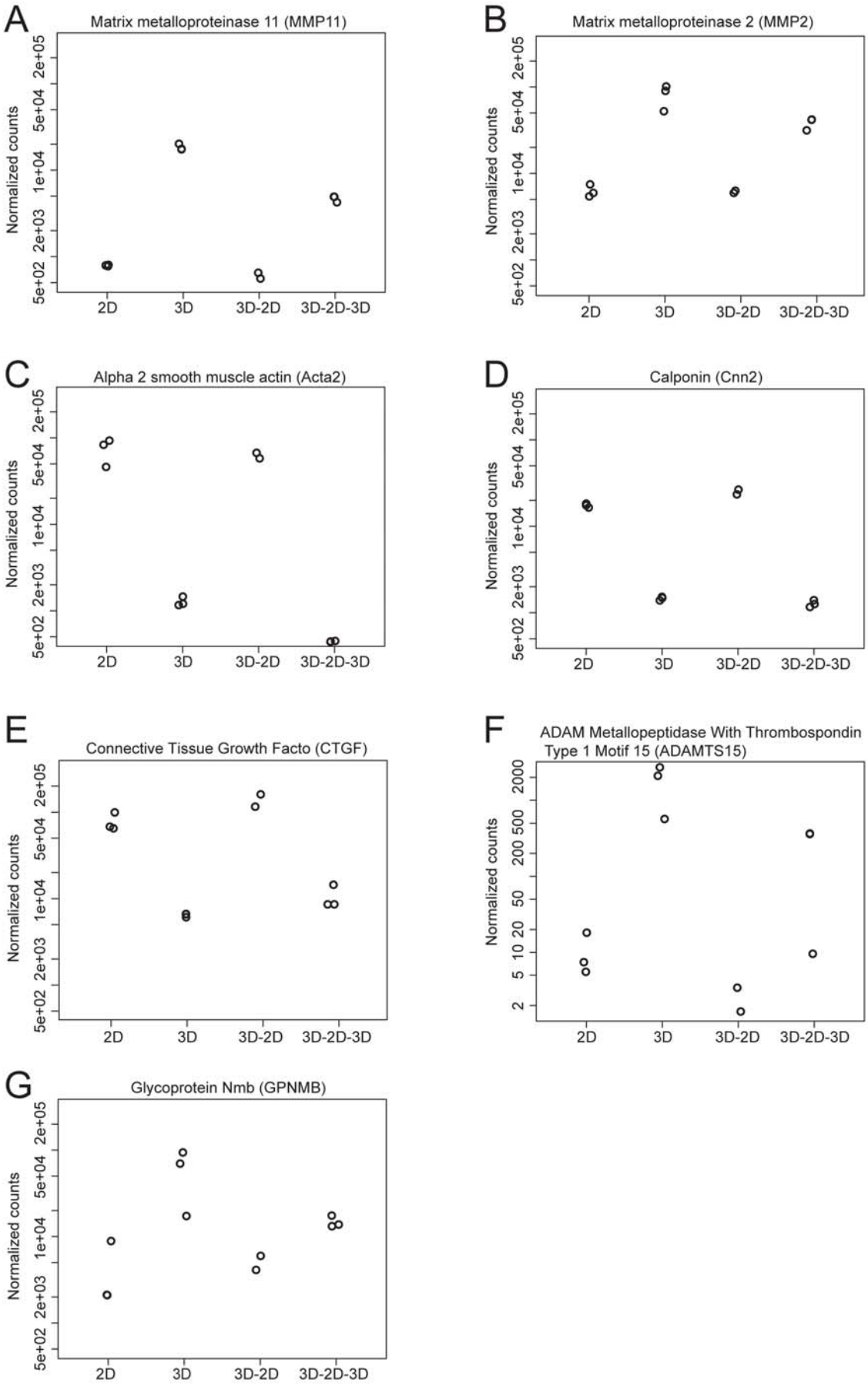

FIGURE 2

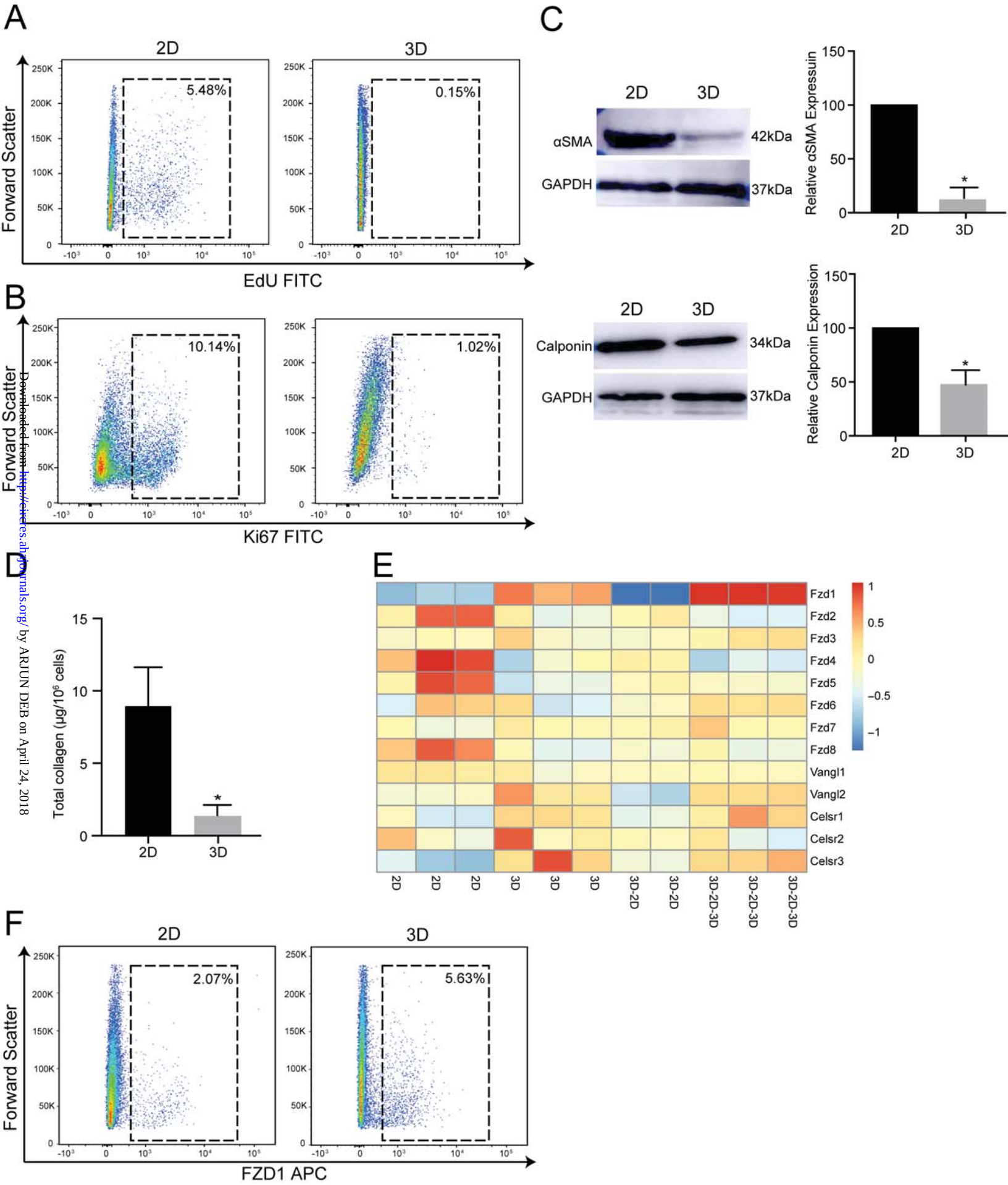

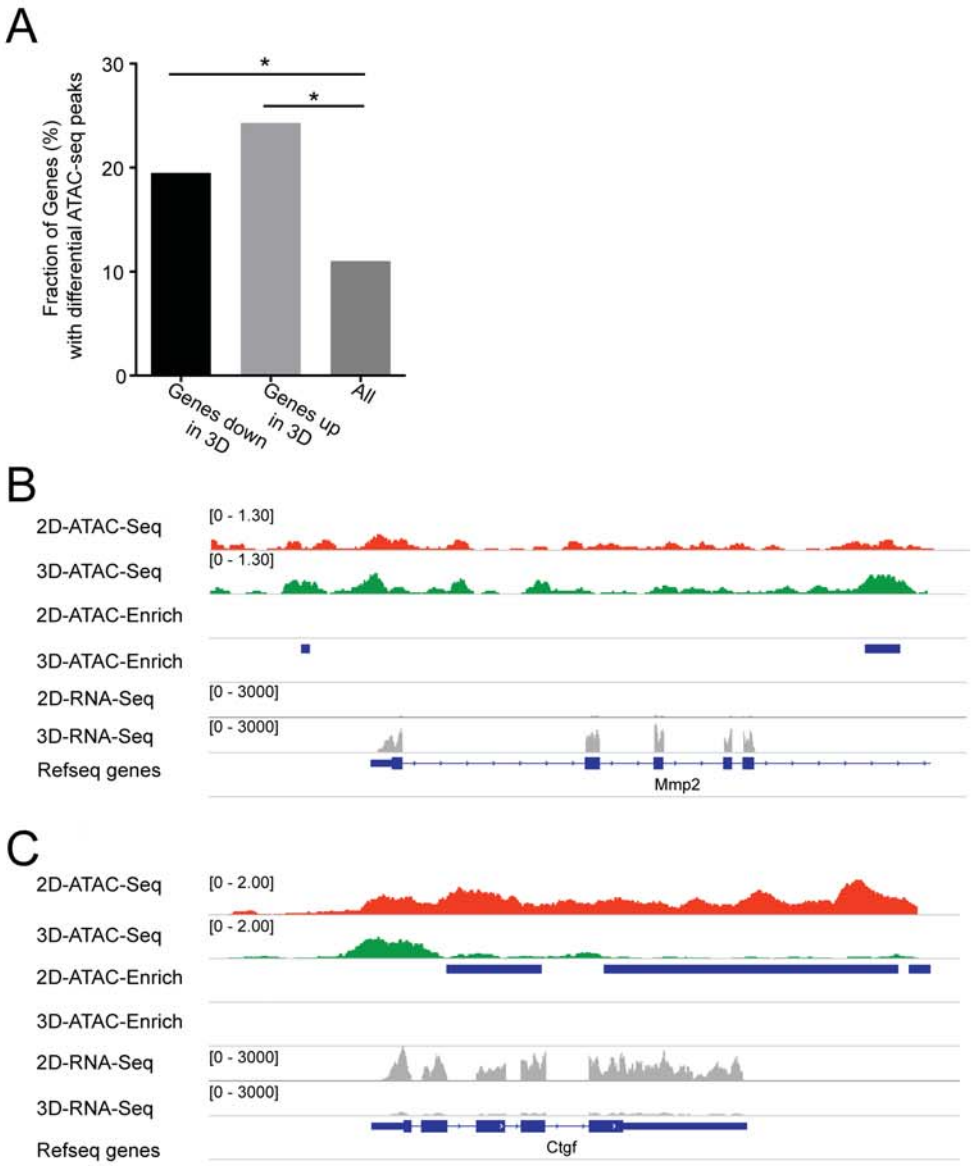

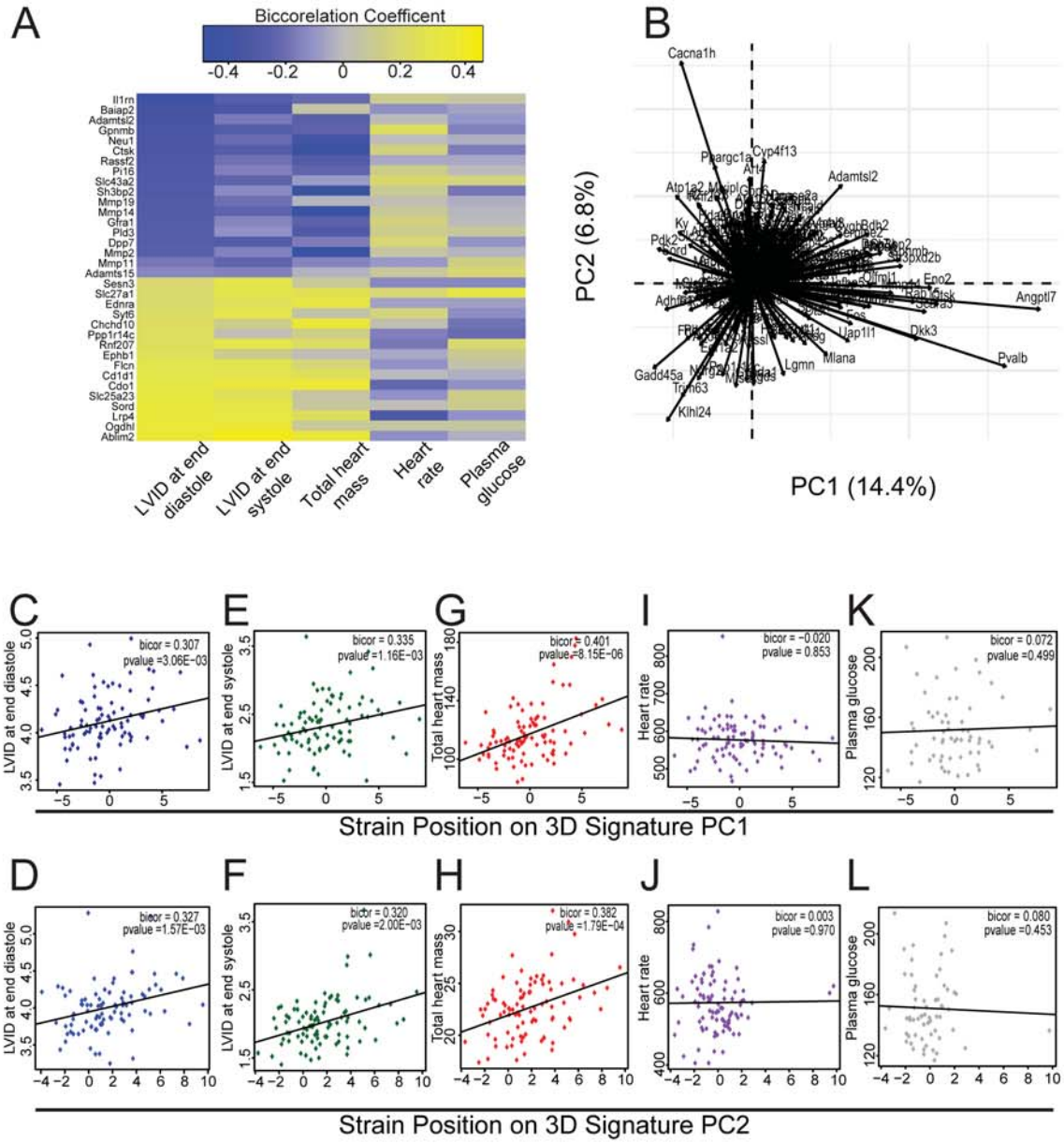

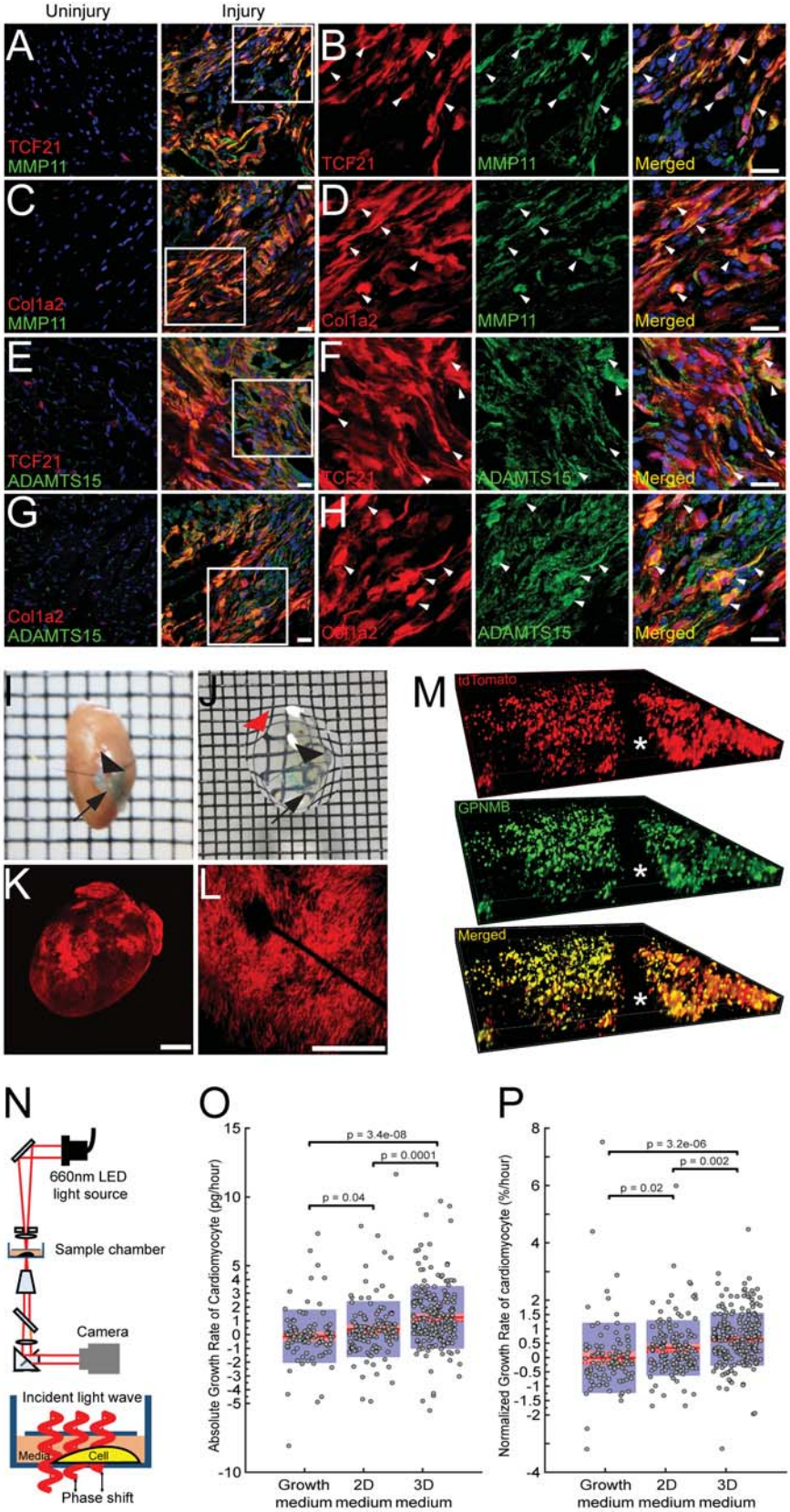

FIGURE 6

Circulation Research
JOURNAL OF THE AMERICAN HEART ASSOCIATION

Topological Arrangement of Cardiac Fibroblasts Regulates Cellular Plasticity

Jingyi YU, Marcus M Seldin, Kai Fu, Shen Li, Larry Lam, Ping Wang, Yijie Wang, Dian Huang, Thang L Nguyen, Bowen Wei, Rajan P Kulkarni, Dino Di Carlo, Michael Teitell, Matteo Pellegrini, Aldons J Lusis and Arjun Deb

Circ Res. published online April 24, 2018;
Circulation Research is published by the American Heart Association, 7272 Greenville Avenue, Dallas, TX 75231

Print ISSN: 0009-7330. Online ISSN: 1524-4571

Supplementary Methods

Animal care and use

All experimental procedures involving animals in this study were approved by the Institutional Animal Care and Use Committee (IACUC) of University of California at Los Angeles (UCLA). All animals were maintained at the UCLA vivarium according to the policies instituted by the American Association for Accreditation of Laboratory Animal Care.

Isolation of cardiac fibroblasts

Cardiac fibroblasts were isolated as described(1, 2). Briefly, cardiac fibroblasts were isolated from explanted hearts of uninjured wild type or Col1a2CreERT:R26R^{tdTomato} and TCF21MerCreMer:R26R^{tdTomato} mice which previously injected with tamoxifen for 10 days. The hearts were explanted and washed three times with 1× HBSS (GIBCO) then minced into approximately 1mm^2 sized pieces and digested using 12.5 ml Liberase TH (SIGMA, CAT# 5401151001) digestion buffer [prepared by adding 5mg of liberase TH to 50ml Tyrodes buffer (136mM NaCl, 5.4mM KCl, 0.33mM NaH_2PO4, 1.0mM $MgCl_2$, 10mM HEPES with 1.8mg/L Glucose) to a final concentration of 0.1ug/ml]. Two sequential digestions were performed at 37°C. The cells were collected and passed through a 40μm strainer and plated in F12K medium (CORNING) with 1% penicillin/streptomycin, 20% Fetal Bovine Serum (FBS) (GIBCO) for 2 h at 37°C in a 5% CO2 incubator. After incubation for 2 hours, the medium was changed to F12K medium (GIBCO) supplemented with 20% FBS, 1% penicillin/streptomycin, 1,000 U/ml leukemia inhibitory factor (LIF) (Millipore) and 10 ng/ml basic fibroblast growth factor (bFGF) (Millipore). Cells were maintained under these conditions until they became confluent and used. All the cardiac fibroblast that had not undergone more than 3 passages were used for experiments

Cardiac fibroblast 2D/3D culture

For cardiac fibroblast sphere formation, the primary outgrowth of confluent monolayer cardiac fibroblasts from C57BL/6J, Col1a2CreERT:R26R^{tdTomato} or TCF21MerCreMer:R26R^{tdTomato} mice were harvested (0.25% trypsin-EDTA) and re-plated onto regular tissue culture dish (2D) (CORNING) or ultra-low attachment dish (3D) (CORNING) (CAT# 3261) at a density of 1-1.2 × 10^5 cells/cm^2. Both 2D and 3D cardiac fibroblasts were treated with identical cell culture medium [35% IMDM, 65% F12K, 3.5% FBS, 1% penicillin-streptomycin, 200mmol/L L-glutamine, 20ng/ml bFGF, 25ng/ml EGF (PEPROTECH), 1,000 U/ml LIF, 0.1mM 2-Mercaptoethanol (SIGMA)](3, 4). Under these conditions, cardiac fibroblasts seeded onto ultra -low attachment plates formed spherical clusters within 24 hours of seeding. After 24 h, the 3D spheres were collected and plated back onto a regular cell culture dish at 37°C 5%CO_2 for 5 days, with cell culture medium being changed every two days. The spherical clusters of cardiac fibroblasts attached and fibroblasts migrated out to form a monolayer by 5 days (3D-2D). Fibroblasts in 2D or 3D states maintained for 5 days served as controls. These cells were subsequently trypsinized and reseeded onto ultra-low attachment plates, where they again formed spherical clusters (3D-2D-3D) within 24 hours. Cells identically trypsinized but reseeded onto 2D conditions served as controls. Cardiac fibroblasts at different topological states were used for RNA-seq and ATAC-seq experiments. For WGS staining, cardiac fibroblasts isolated from Col1a2CreERT:R26R^{tdTomato} and TCF21MerCreMer: R26R^{tdTomato} were fixed in 2% paraformaldehyde for 15 min at 37˚C, then stained with 1:200 diluted Wheat Germ Agglutinin Conjugates (WGA) stock solution 1.0mg/mL (Invitrogen) in HBSS for 10 min at room temperature (5). The cells were subsequently washed twice with HBSS and then permeabilized with 0.2% Triton X-1000 for 15min. Finally, the cells were mounted in slow fade gold anti-fade reagent with DAPI. Labeled cells were imaged with a confocal microscope (PROMO C2, NIKON).

To determine changes in gene expression of cardiac fibroblasts seeded onto substrates with varying elastic moduli (stiffness), cardiac fibroblasts ($5x10^5$ cells) were cultured on 6-well plates with various rigidities (0.5, 8, 64 kPa) at 37˚C, 5%CO_2 for 24 hours according to the manufacturer's instruction (Advanced BioMatrix, CAT# 5145) (5, 6). All wells were pre-coated with type I collagen according to manufacturer's instructions (100μg/ml collagen Type I). Cardiac fibroblasts seeded onto regular tissue culture dishes precoated with type I collagen and at a similar seeding density served as controls. Cardiac fibroblasts seeded onto ultra-low attachment plates were used to create 3D fibroblast states for analyzing gene expression changes within the different groups. Following 24 hours of seeding, cells were harvested for RNA-seq.

RNA-seq and ATAC-seq

RNA was isolated from cardiac fibroblasts in different topological states, temporally adjusted controls as well as from cardiac fibroblasts seeded onto substrates of varying elastic moduli (0.5, 8, 64 kPa). RNA isolation was performed using PROMEGA RNA Isolation Kit (PROMEGA) and reverse transcription using Reverse Transcription System (PROMEGA). Libraries were constructed using standard Illumina RNA-seq library construction protocols and were sequenced on Illumina HiSeq 3000. For analysis of gene expression changes, we first mapped RNA-Seq reads of each sample to its corresponding genomic coordinates (mm10 genome version) with Tophat software (default parameters)(7). Next, we quantified the expression of each gene, i.e. the number of reads falling into each gene, with HTSeq-count software(8). We then performed the normalization and differential expressed genes (DEGs) analysis with DESeq2 software(9). The identified DEGs required a FDR value smaller than 0.01 and a log2 fold change larger than 1. Marker set enrichment analysis (MSEA) was performed on the DESeq2 output from RNA-sequencing, based on normalized fold-change expression in 3D/2D (3D up-regulated) and 2D/3D (3D down-regulated) conditions as well as for fibroblasts on substrates of varying stiffness. For pathway analysis, genes in each condition were weighted based on their fold-change, merged into modules based on Gene Ontology Terms and permuted 2000 times against transcripts detected across all RNA-seq samples to generate corresponding p-values(9, 10).

ATAC-seq was performed as described previously(11) using approximately 50,000 cells/sample. Cardiac fibroblasts harvested from all topological states (2D, 3D) were subjected to ATAC-seq. Samples were lysed with cold lysis buffer (10 mM Tris-HCl, pH 7.4, 10 mM NaCl, 3 mM $MgCl_2$ and 0.1% IGEPAL CA-630). Immediately following the nuclei preparation, the pellets were re-suspended in the transposase reaction mix (25μl 2×TD buffer, 2.5μl transposase (Illumina) and 22.5μl nuclease-free water). The transposition reaction was carried out for 30 min at 37°C. Directly following transposition, the samples were purified using a Qiagen MinElute kit. Following purification, the libraries were amplified using 1×NEB next PCR master mix and 1.25μM of custom Nextera PCR primers 1 and 2 (**Table 1**), using the following PCR conditions: 72°C for 5min; 98°C for 30 s; and thermocycling at 98°C for 10 s, 63°C for 30 s and 72°C for 1 min. Libraries were purified using a Qiagen PCR cleanup kit yielding a final library concentration of ~30nM in 20μl to remove primer dimers. Libraries were amplified for a total of 10–12 cycles. For analysis of ATAC-seq data, we first mapped ATAC-Seq reads of each sample to its corresponding genomic coordinates with Bowtie2 software, requiring no more than two mismatches(12). The uniquely mapped reads were then used for further analyses. We used MACS2 software to identify the enriched signal regions of ATAC-Seq peaks with default q-value cutoff(13). To compare the ATAC-Seq signals between different samples, we used MACS2 bdg diff function, requiring the identified differential regions were having a log10 likelihood of more than 5.

Expression overlay with hybrid mouse diversity panel

Differentially expressed transcripts from 2D vs 3D spheres were used for population-based analysis within the HMDP. We utilized gene expression arrays from left ventricle (GEO accession: GSE48760) among HMDP strains subjected to isoproterenol treatment. ALZET Model 1004 minipumps (Cupertino, CA, USA) were implanted intra-peritoneally to administered ISO, at a dose of 30 mg/kg body weight/day for 21 days. At the end of the protocol, mice were sacrificed by giving a sub-lethal dosage of inhaled isoflurane followed by cervical dislocation. LV tissues were collected and frozen immediately in liquid nitrogen. Data from HMDP populations administered isoproterenol were analyzed from the following studies(14, 15). From these arrays, all probes corresponding to the same genes were aggregated to a single gene by strain measurement. This gene-by-strain matrix was used for further analyses. Initially, individual differentially expressed genes were correlated with clinical traits from the corresponding isoproterenol study. For a larger sample size and consistency, we chose to measure echocardiogram traits following 14 days of isoproterenol infusion. Biweight midcorrelation values (bicor) were calculated using pairwise strains (70-96, depending on the trait assessed) in the R package WGCNA(16). From the matrix of gene-by-trait, biweight midcorrelation coefficients student p-values were calculated using the corresponding sample sizes. Following individual gene x trait correlations, the gene -by-strain matrix from HMDP study was used for eigengene construction. First, the matrix was narrowed down to genes only upregulated under 3D conditions by overlaying gene symbol of aggregated probes with the output from DESeq2 analysis on 3D fibroblast spheres. Next principal component analysis was performed on the remaining gene set (R package, prcomp) and score contributions for components were extracted for each strain. The score matrices for each PC and strain were then correlated against traits also using WGNCA as described above.

Flow cytometry analysis

Cultured Cardiac fibroblasts at different topological states were dissociated using 0.25% trypsin-EDTA solution (SIGMA), stained in FACS buffer (0.1%BSA PBS) with APC-conjugated anti-Frizzled-1 antibody (Miltenyi Biotec Inc. cat#130-112-398) or FITC conjugated anti-Ki67 antibody (eBioscience, cat#11-5698-82) for 30min at 4°C. After washing with FACS buffer twice, stained cells were analyzed on a flow cytometer. Unstained control cells were run first to establish gates followed by the cells stained with the primary antibody conjugated to the fluorophore. For EdU analysis, EdU was added to the cell culture medium at a final concentration of 10mM. After 4 hours incubation, the cells were dissociated with 0.25% trypsin-EDTA solution; cells were then fixed and permeabilized with 1x Click-iT saponin-based permeabilization and wash regent for 15min according to the manufacturing instruction of Click-iT™ Plus EdU Alexa Fluor™ 488 Flow Cytometry Assay Kit (Life technologies, cat#C10632). Subsequently Click-iT reaction cocktail was added to the cells and incubated for an additional 30 minutes at room temperature. After washing with1x Click-iT saponin-based permeabilization and wash regent twice, cells were analyzed on a flow cytometer.

Cell Cycle analysis using ImageStream

Cultured Cardiac fibroblasts at different topological states were dissociated as described above and fixed with 1% PFA on ice for 20min. Cells were washed twice with PBS/2%FBS twice, and then passed through a 70µm nylon mesh strainer. At least 1 million cells in 50µl were used for flowcytometry analyzing on the ImageStream system with bright field at 40x magnification (Amnis). Parameters including cell image, cell diameter, cell surface area were analyzed (n=3000 cells used for analysis) using the IDEAS™ post-acquisition analysis software (Amnis) (17, 18).

Immunoblotting analysis

Cultured Cardiac fibroblasts at different topological states were washed twice with ice-cold PBS and harvested in RIPA Lysis and Extraction Buffer (life technologies) plus Halt Protease Inhibitor Cocktail (life technologies) and Halt™ Phosphatase Inhibitor Cocktail (life technologies). Pierce™ BCA Protein Assay Kit was used for the colorimetric detection and quantitation of total protein (Life Technologies). Total 25μg protein was separated on 4-12% Tris-Glycine Mini Gels (Life Technologies) and transferred onto PVDF membranes (Merck Millipore). The membranes were probed with antibodies to alpha smooth muscle Actin (α SMA, 1:1000) (Abcam, cat# ab5694), calponin(1:1000)(Abcam, cat# ab46794), GAPDH(1:5000) (MilliporeSigma, cat# ABS16). Protein signals were detected using horseradish peroxidase (HRP)-conjugated secondary antibodies and enhanced chemiluminescence (ECL) western blotting detection regents (Thermo Fisher Scientific, MA, USA).

Sircol assay for determining collagen amounts

The Sircol collagen assay kit (Biocolor Ltd.,Newtownabbey, UK, CAT# CLRS4000) was used to quantify total collagen amounts in cardiac fibroblasts in 2D or 3D states according to the manufacturer's instructions. Collagen was measured only in 2D or 3D fibroblasts following harvest and collagen secreted from the cells onto the surface of the dish was thus not measured in this assay. In brief, collagen was extracted and digested overnight with 0.1 mg/ml pepsin in 5 M acetic acid. Soluble and insoluble collagen was measured according to the manufacturer's instructions using a standard curve of known concentrations of purified rat tail collagen to estimate total collagen content (19, 20).

Genetic labeling of cardiac fibroblasts

Col1a2CreERT:R26R^{tdTomato} and TCF21MerCreMer:R26R^{tdTomato} mice lines were obtained by crossing Collagen1a2CreERT and TCF21MerCreMer mice with the lineage reporter R26R ^{tdTomato} mice(1). Tamoxifen (1mg) (Sigma) was injected intraperitoneally for 10 days to induce Cre-mediated recombination in Col1a2CreERT:R26R^{tdTomato} and TCF21MerCreMer:R26R^{tdTomato} mice (8-10 weeks old). Five days following cessation of tamoxifen, animals were subjected to cardiac fibroblasts isolation or cardiac injury (myocardial cryoinjury). All mice were maintained on a C57BL/6 background. For isolation of tdTomato labeled cardiac fibroblasts, cultured cardiac fibroblasts isolated from non-transgenic mice were first run through the flow cytometer to establish gates. Next population of cultured cardiac fibroblasts isolated from Col1a2CreERT:R26R^{tdTomato} or TCF21MerCreMer:R26R^{tdTomato} mice hearts were run through the same gates to identify tdTomato labeled cells. All the tdTomato labeled cardiac fibroblast were sorted and collected for further culture and assays.

Murine Cardiac Cryo-injury

Mice (both male and female), 8–10 weeks old, were subjected to sham or myocardial cryoinjury as described(1). For cryoinjury, mice were initially anaesthetized with 3% isoflurane, maintained at 2% isoflurane, and intubated using a Harvard Rodent Volume-Cycled ventilator. A left thoracotomy was performed at the level of 2nd intercostal space and cardiac cryo-injury was performed by gently pressing a steel rod of 1mm diameter pre-cooled in dry ice against the exposed beating heart for 10 seconds. Freezing of cardiac tissue was confirmed by the rapid discoloration of the tissue. Seven days after injury, the hearts were harvested and processed for histological analysis.

Immunofluorescent staining and confocal microscopy

For harvesting the heart, the left ventricle was perfused with 5 ml PBS followed by 2 ml of 4%

paraformaldehyde (PFA). The hearts were post fixed in 4% PFA for additional 4 h and cryo-protected using 25% sucrose and embedded in OCT compound (TISSUE-TEK) (1). Immunofluorescent staining was performed on 7 mm frozen sections against markers that were upregulated in 3D spheres. Sections were washed and blocked using 10% normal donkey serum for 1 h and then stained with primary antibodies against MMP11 (ABCAM, AB119284), ADAMTS15 (R&D STSTEMS, AF5149) overnight at 4°C. After washing three times with PBS, sections were incubated in secondary antibodies for 1 h followed by washing an additional three times with PBS. Finally, the sections were mounted in slow fade gold anti-fade reagent with DAPI (LIFT TECHNOLOGIES, S36938). Labeled sections were imaged using a PROMO C2 inverted Laser Scanning Confocal Microscope (NIKON). For each sample, eight independent images within 100mm radius of the cryo injured region were used for quantitative analysis.

Mouse Heart Clearing using simplified CLARITY method (SCM) and Immunofluorescence Labeling

A simplified CLARITY method was used to perform cardiac tissue clearing as described(21). Mouse hearts were rinsed thoroughly with 1x Phosphate Buffered Saline (PBS) immediately following harvesting to remove residual blood from cardiac chambers. The hearts were subsequently fixed in 4% paraformaldehyde (PFA) overnight at 4°C. Following fixation, samples were rinsed with 1x PBS and then immersed in a solution of 4% acrylamide monomer (Bio-Rad) along with 0.625% w/v of the photoinitiator 2,2'-Azobis[2-(2-imidazolin-2-yl) propane] dihydrochloride (VA-044, Wako Chemicals USA). The tissues were then incubated overnight at 4°C. The following day, the tubes containing the hearts were incubated at 37°C for 3-4 hours, until the acrylamide solution became viscous. After polymerization, the tissues were rinsed with 1x PBS and then placed into a clearing solution comprised of 8% w/v sodium dodecyl sulfate (SDS, Sigma Aldrich) and 1.25% w/v boric acid (Fischer) (Ph8.4). Samples were incubated at 37°C until the desired transparency was reached, usually two weeks. Following incubation in clearing solution, the heart samples were washed with 1x PBS for one day and then blocked with bovine serum albumin (1x PBS, 1% BSA, 0.05% Tween-20) overnight prior to immunofluorescence applications. For immunofluorescence studies, the heart samples were incubated with GPNMB (R&D Systems, AF2550) primary antibody at 1:100 dilution for 24 hours. Samples were then rinsed with PBS for one day prior to the application of the appropriate Alexa 488-conjugated secondary antibody (Cell Signaling) for 24 hours at 1:100 dilution. To amplify the endogenous tdTomato signal when present, anti-td-Tomato primary antibody (Rockland) and appropriate Alexa 555-conjugated secondary antibody (Cell Signaling) were applied as described above. Following immunofluorescence labeling, the heart samples were placed in Refractive Index Matching Solution (RIMS) prior to imaging. To make 30 mL RIMS, 40 grams of Histodenz (Sigma-Aldrich) was dissolved in 1X PBS (Sigma) with 0.05% w/v sodium azide (Sigma) and syringe filtered through a 0.2 μm filter.

2D/3D conditioned medium experiments on neonatal rat ventricular myocytes

NRVMs were isolated from P1-P3 day old Sprague-Dawley rat pups of mixed gender as described previously (22) and plated with 700ul plating medium (DMEM, supplemented with 10% FBS and 1% penicillin/streptomycin) in a μ–Slide 4 well Ph+ (Phase contrast plus) (IBIDI) coated with 0.1% gelatin (104 cells /well). After resting overnight in plating medium, medium was changed to 700ul serum-free DMEM medium supplemented with 1% insulin-transferrin-selenium (ITS) (BD BIOSCIENCE) and 1% penicillin/streptomycin. Cells were incubated at 37°C, 5% CO_2. The medium was then replaced with conditioned medium obtained from 2D or 3D cardiac fibroblast cultures and myocyte mass measured over the next 48 hours.

Live cell Interferometry (LCI)

Cells were imaged every 30 min for up to 48 hours at 20x magnification using a 0.40 numerical aperture objective on an Axio Observer.A1 inverted microscope (Zeiss) in a temperature and CO2 regulated stage-

top cell incubation chamber. Quantitative phase microscopy (QPM) data was captured with a quadriwave lateral shearing interferometry (QWLSI) camera (SID4BIO, Phasics)(23). Illumination was provided by a 660nm center wavelength collimated LED (Thorlabs). In each experiment, QPM data was collected from 32 distinct locations for automated image processing and biomass segmentation analysis.

Quantitative phase microscopy (QPM) image analysis

All images were processed with custom MATLAB (MathWorks) scripts. Cells were identified and segmented using a local adaptive threshold based on Otsu's method (24) and tracked using particle tracking code based on Grier et al (25).

Biomass accumulation rate calculation

QPM biomass data was summed over the projected area of each cell to obtain total cell biomass at each collection time point. Biomass accumulation rates were calculated by fitting a first-order polynomial to each biomass versus time plot using MATLAB Polyfit (Math Works). Individual cell growth tracks were quality filtered using an upper cutoff of ± 5% uncertainty (s.d. of residuals) in the calculated growth rate, as determined by linear fitting the biomass versus time data.

Statistics

All data are presented as mean± standard error of the mean (S.E.M.). The value of n stated in the figure legends stands for independent biological replicates. Statistical analysis was performed using Graph Pad (Prizm) using student's t-test (two tailed). A P value <0.05 was considered significant and individual p values are mentioned in the figure/figure legend.

All computational procedures were carried out using R statistical software. For analysis of the Hybrid Mouse Diversity Panel (HMDP) and correlation of phenotypic traits with 3D upregulated genes, all computational procedures were carried out using R statistical software. The HMDP expression arrays were aggregated to average expression of each gene across multiple probes and used for correlation or principal component analysis. Correlations and associated p-values were calculated with the biweight midcorrelation, which is robust to outliers and associated pvalue (16). Principle component vectors were assigned using the R base function "prcomp" where strain position on corresponding vectors were used for correlation analysis also using WGCNA. Transcriptional Regulatory Relationships Unraveled by Sentence-based Text mining (TRRUSTv2) were interrogated for literature-based transcription factor (TF)-target interactions which persist in mice, focused on significance (FDR < 0.1) of TFs enriched among interactions with the set of 3D-enriched genes. Single comparisons between two groups were performed using two-tailed Student's *t* tests with 95% confidence intervals. To retrieve and overlay annotated secreted proteins, we used the list deposited in the Universal Protein resource (UniProt) as "secreted" localization annotations [SL-0243] for overlapping HUGO symbol in Mus musculus (Mouse) [10090].

Table 1: Oligo designs. A list of ATAC-seq oligos used for PCR.

Ad1_noMX:	AATGATACGGCGACCACCGAGATCTACACTCGTCGGCAGCGTCAGATGTG
Ad2.1_TAAGGCGA	CAAGCAGAAGACGGCATACGAGATTCGCCTTAGTCTCGTGGGCTCGGAGATGT
Ad2.2_CGTACTAG	CAAGCAGAAGACGGCATACGAGATCTAGTACGGTCTCGTGGGCTCGGAGATGT
Ad2.3_AGGCAGAA	CAAGCAGAAGACGGCATACGAGATTTCTGCCTGTCTCGTGGGCTCGGAGATGT
Ad2.4_TCCTGAGC	CAAGCAGAAGACGGCATACGAGATGCTCAGGAGTCTCGTGGGCTCGGAGATGT
Ad2.5_GGACTCCT	CAAGCAGAAGACGGCATACGAGATAGGAGTCCGTCTCGTGGGCTCGGAGATGT
Ad2.6_TAGGCATG	CAAGCAGAAGACGGCATACGAGATCATGCCTAGTCTCGTGGGCTCGGAGATGT
Ad2.7_CTCTCTAC	CAAGCAGAAGACGGCATACGAGATGTAGAGAGGTCTCGTGGGCTCGGAGATGT
Ad2.8_CAGAGAGG	CAAGCAGAAGACGGCATACGAGATCCTCTCTGGTCTCGTGGGCTCGGAGATGT
Ad2.9_GCTACGCT	CAAGCAGAAGACGGCATACGAGATAGCGTAGCGTCTCGTGGGCTCGGAGATGT
Ad2.10_CGAGGCTG	CAAGCAGAAGACGGCATACGAGATCAGCCTCGGTCTCGTGGGCTCGGAGATGT
Ad2.11_AAGAGGCA	CAAGCAGAAGACGGCATACGAGATTGCCTCTTGTCTCGTGGGCTCGGAGATGT
Ad2.12_GTAGAGGA	CAAGCAGAAGACGGCATACGAGATTCCTCTACGTCTCGTGGGCTCGGAGATGT
Ad2.13_GTCGTGAT	CAAGCAGAAGACGGCATACGAGATATCACGACGTCTCGTGGGCTCGGAGATGT
Ad2.14_ACCACTGT	CAAGCAGAAGACGGCATACGAGATACAGTGGTGTCTCGTGGGCTCGGAGATGT
Ad2.15_TGGATCTG	CAAGCAGAAGACGGCATACGAGATCAGATCCAGTCTCGTGGGCTCGGAGATGT
Ad2.16_CCGTTTGT	CAAGCAGAAGACGGCATACGAGATACAAACGGGTCTCGTGGGCTCGGAGATGT
Ad2.17_TGCTGGGT	CAAGCAGAAGACGGCATACGAGATACCCAGCAGTCTCGTGGGCTCGGAGATGT
Ad2.18_GAGGGGTT	CAAGCAGAAGACGGCATACGAGATAACCCCTCGTCTCGTGGGCTCGGAGATGT
Ad2.19_AGGTTGGG	CAAGCAGAAGACGGCATACGAGATCCCAACCTGTCTCGTGGGCTCGGAGATGT
Ad2.20_GTGTGGTG	CAAGCAGAAGACGGCATACGAGATCACCACACGTCTCGTGGGCTCGGAGATGT
Ad2.21_TGGGTTTC	CAAGCAGAAGACGGCATACGAGATGAAACCCAGTCTCGTGGGCTCGGAGATGT
Ad2.22_TGGTCACA	CAAGCAGAAGACGGCATACGAGATTGTGACCAGTCTCGTGGGCTCGGAGATGT
Ad2.23_TTGACCCT	CAAGCAGAAGACGGCATACGAGATAGGGTCAAGTCTCGTGGGCTCGGAGATGT
Ad2.24_CCACTCCT	CAAGCAGAAGACGGCATACGAGATAGGAGTGGGTCTCGTGGGCTCGGAGATGT

Supplemental References

1. Pillai IC, Li S, Romay M, Lam L, Lu Y, Huang J, et al. Cardiac Fibroblasts Adopt Osteogenic Fates and Can Be Targeted to Attenuate Pathological Heart Calcification. *Cell stem cell.* 2017;20:218-32 e5.
2. Pinz I, Zhu M, Mende U, and Ingwall JS. An improved isolation procedure for adult mouse cardiomyocytes. *Cell Biochem Biophys.* 2011;61:93-101.
3. Wang YJ, Bailey JM, Rovira M, and Leach SD. Sphere-forming assays for assessment of benign and malignant pancreatic stem cells. *Methods Mol Biol.* 2013;980:281-90.
4. Chen L, Pan Y, Zhang L, Wang Y, Weintraub N, and Tang Y. Two-step protocol for isolation and culture of cardiospheres. *Methods Mol Biol.* 2013;1036:75-80.
5. Gutierrez E, and Groisman A. Measurements of elastic moduli of silicone gel substrates with a microfluidic device. *PLoS One.* 2011;6:e25534.
6. Prager-Khoutorsky M, Lichtenstein A, Krishnan R, Rajendran K, Mayo A, Kam Z, et al. Fibroblast polarization is a matrix-rigidity-dependent process controlled by focal adhesion mechanosensing. *Nature cell biology.* 2011;13:1457-65.
7. Trapnell C, Roberts A, Goff L, Pertea G, Kim D, Kelley DR, et al. Differential gene and transcript expression analysis of RNA-seq experiments with TopHat and Cufflinks. *Nature protocols.* 2012;7:562-78.
8. Anders S, and Huber W. Differential expression analysis for sequence count data. *Genome biology.* 2010;11:R106.
9. Arneson D, Bhattacharya A, Shu L, Makinen VP, and Yang X. Mergeomics: a web server for identifying pathological pathways, networks, and key regulators via multidimensional data integration. *BMC genomics.* 2016;17(1):722.
10. Shu L, Zhao Y, Kurt Z, Byars SG, Tukiainen T, Kettunen J, et al. Mergeomics: multidimensional data integration to identify pathogenic perturbations to biological systems. *BMC genomics.* 2016;17:874.
11. Buenrostro JD, Giresi PG, Zaba LC, Chang HY, and Greenleaf WJ. Transposition of native chromatin for fast and sensitive epigenomic profiling of open chromatin, DNA-binding proteins and nucleosome position. *Nature methods.* 2013;10:1213-8.
12. Langmead B, and Salzberg SL. Fast gapped-read alignment with Bowtie 2. *Nature methods.* 2012;9(4):357-9.
13. Zhang Y, Liu T, Meyer CA, Eeckhoute J, Johnson DS, Bernstein BE, et al. Model-based analysis of ChIP-Seq (MACS). *Genome biology.* 2008;9:R137.
14. Rau CD, Wang J, Avetisyan R, Romay MC, Martin L, Ren S, et al. Mapping genetic contributions to cardiac pathology induced by Beta-adrenergic stimulation in mice. *Circulation Cardiovascular genetics.* 2015;8:40-9.
15. Wang JJ, Rau C, Avetisyan R, Ren S, Romay MC, Stolin G, et al. Genetic Dissection of Cardiac Remodeling in an Isoproterenol-Induced Heart Failure Mouse Model. *PLoS genetics.* 2016;12:e1006038.
16. Langfelder P, and Horvath S. Eigengene networks for studying the relationships between co-expression modules. *BMC Syst Biol.* 2007;1:54.

17. Basiji DA, Ortyn WE, Liang L, Venkatachalam V, and Morrissey P. Cellular image analysis and imaging by flow cytometry. *Clin Lab Med.* 2007;27:653-70, viii.

18. Hennig H, Rees P, Blasi T, Kamentsky L, Hung J, Dao D, et al. An open-source solution for advanced imaging flow cytometry data analysis using machine learning. *Methods.* 2017;112:201-10.

19. Shen C, Jiang L, Shao H, You C, Zhang G, Ding S, et al. Targeted killing of myofibroblasts by biosurfactant di-rhamnolipid suggests a therapy against scar formation. *Sci Rep.* 2016;6:37553.

20. Chu H, Shi Y, Jiang S, Zhong Q, Zhao Y, Liu Q, et al. Treatment effects of the traditional Chinese medicine Shenks in bleomycin-induced lung fibrosis through regulation of TGF-beta/Smad3 signaling and oxidative stress. *Sci Rep.* 2017;7:2252.

21. Sung K, Ding Y, Ma J, Chen H, Huang V, Cheng M, et al. Simplified three-dimensional tissue clearing and incorporation of colorimetric phenotyping. *Sci Rep.* 2016;6:30736.

22. Ota A, Zhang J, Ping P, Han J, and Wang Y. Specific regulation of noncanonical p38alpha activation by Hsp90-Cdc37 chaperone complex in cardiomyocyte. *Circ Res.* 2010;106:1404-12.

23. Bon P, Maucort G, Wattellier B, and Monneret S. Quadriwave lateral shearing interferometry for quantitative phase microscopy of living cells. *Opt Express.* 2009;17:13080-94.

24. Zangle TA, Chun J, Zhang J, Reed J, and Teitell MA. Quantification of biomass and cell motion in human pluripotent stem cell colonies. *Biophys J.* 2013;105::593-601.

25. Zangle TA, Burnes D, Mathis C, Witte ON, and Teitell MA. Quantifying biomass changes of single CD8+ T cells during antigen specific cytotoxicity. *PLoS One.* 2013;8::e68916.

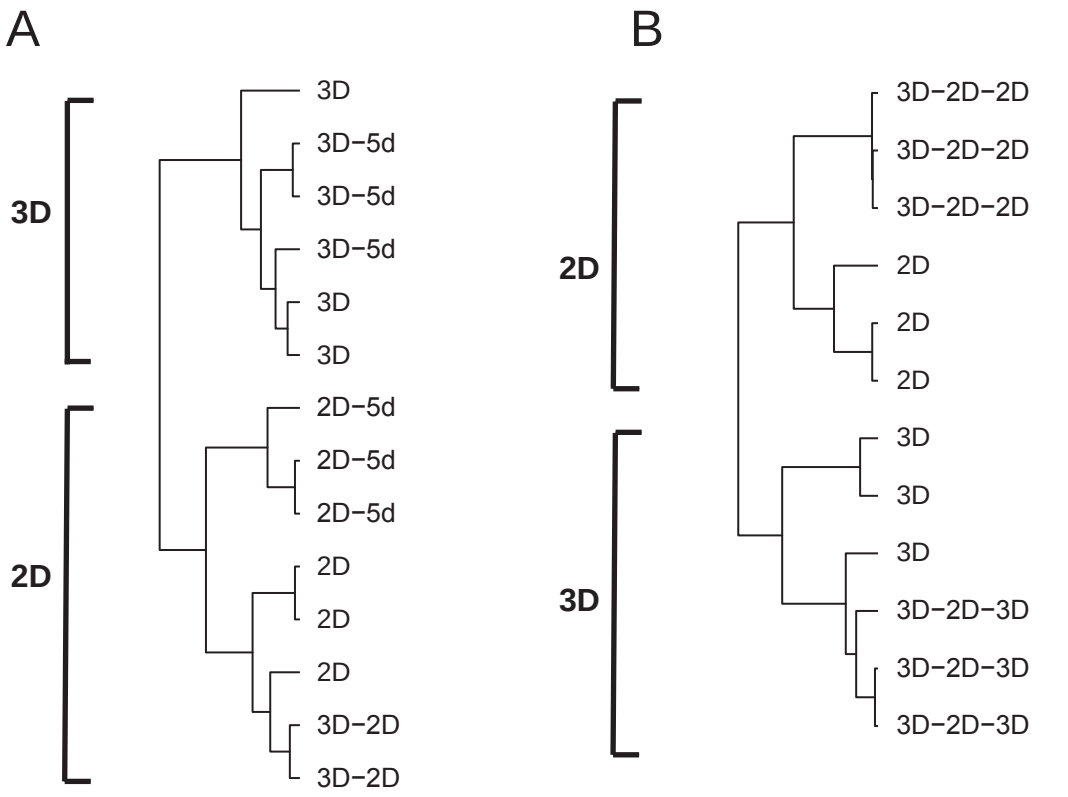

Online Figure I. Dendrogram demonstrating relationship of gene expression patterns of 3D-2D and 3D-2D-3D cardiac fibroblasts with temporally adjusted controls. (A) 3D-2D cardiac fibroblasts were generated by transferring the 3D cardiac fibroblasts to 2D conditions and maintaining the cells for 5 days (allowing the cells to migrate out from spheroids to a monolayer). For this purpose, additional temporally adjusted controls of 2D fibroblasts and 3D fibroblasts maintained in culture for 5 days (2D-5d; 3D-5d) and then subsequently harvested for RNA-seq were used. RNA-seq and gene expression analysis to construct dendrograms shows clustering of 3D-2D groups with 2D and 2D-5 day groups and are distinct from that of 3D or 3D-5 day groups. **(B)** Similarly, 3D-2D-3D fibroblasts were generated by transferring 3D-2D fibroblasts to an ultra-low attachment dish and harvesting the cells at 24 hours after initial seeding. A temporally adjusted control was generated by transferring the 3D-2D cells to a regular tissue culture dish and harvested 24 hours after seeding (3D-2D-2D). Dendrogram again shows clustering of the 3D-2D-3D gene expression pattern with that of the 3D and distinct from the 2D or 3D-2D-2D groups.

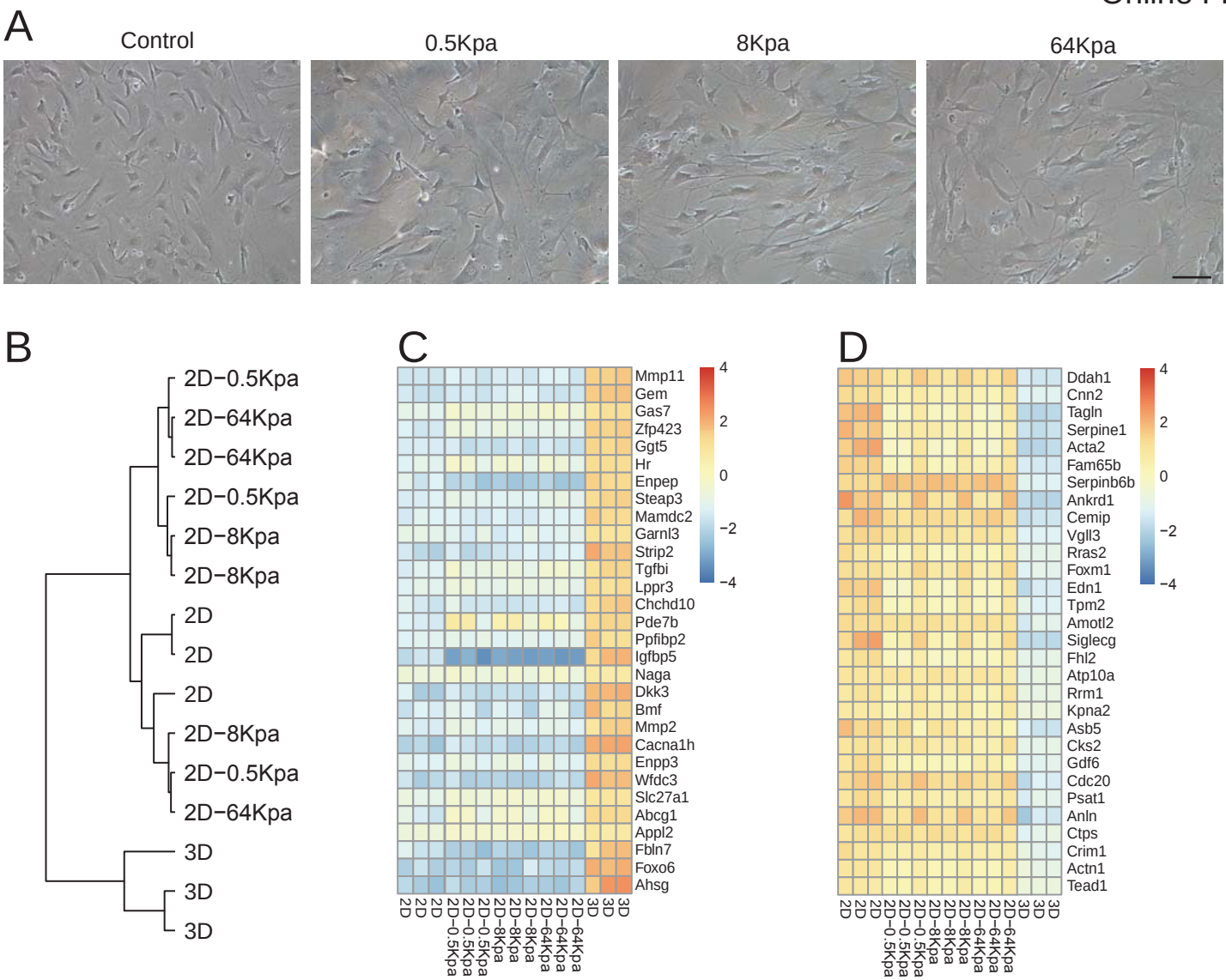

Online Figure II. Gene expression changes following seeding of cardiac fibroblasts onto tissue culture plates with stiffness of 0.5,8 and 64kPa. (A) Cardiac fibroblasts were seeded onto control (regular tissue culture plate or 2D group) or plates of 0.5kPA, 8kPa and 64kPa stiffness or ultra-low attachment plate (3D group) and cells harvested after 24 hours and RNA-seq performed. **(B)** Gene expression analysis and dendrogram demonstrates that the gene expression patterns of cardiac fibroblasts under different stiffness cluster together with that of the 2D group and are distinct from that of the 3D group. **(C,D)** Heat map demonstrating expression of the most highly **(C)** upregulated and **(D)** downregulated genes between the 3D and 2D groups across all the groups.

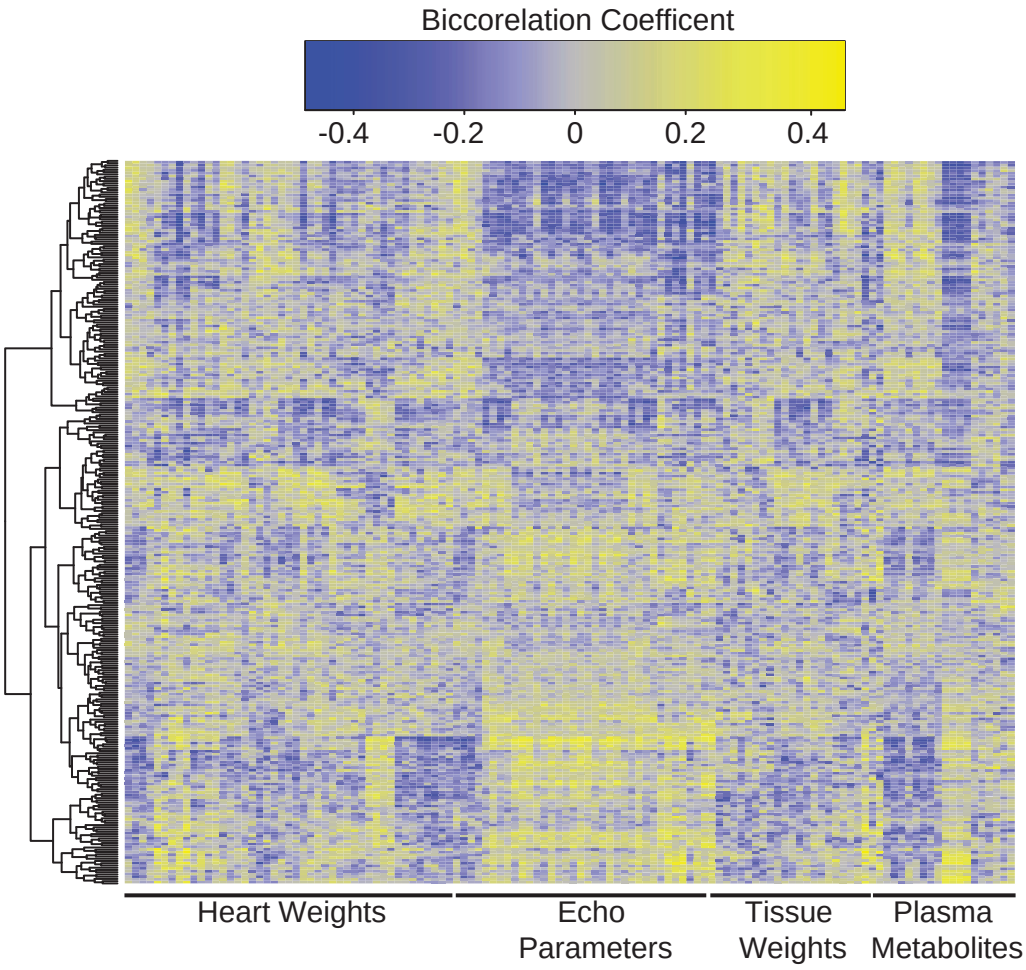

Online Figure III. Heat map of all 3D upregulated genes plotted against all cardiac and non-cardiac traits measured following infusion of isoproterenol in 96 strains of mice. Correlation heat map (yellow: positive and blue: negative correlation) of all differentially upregulated genes in 3D/2D states versus all cardiac and non-cardiac traits following infusion of isoproterenol.

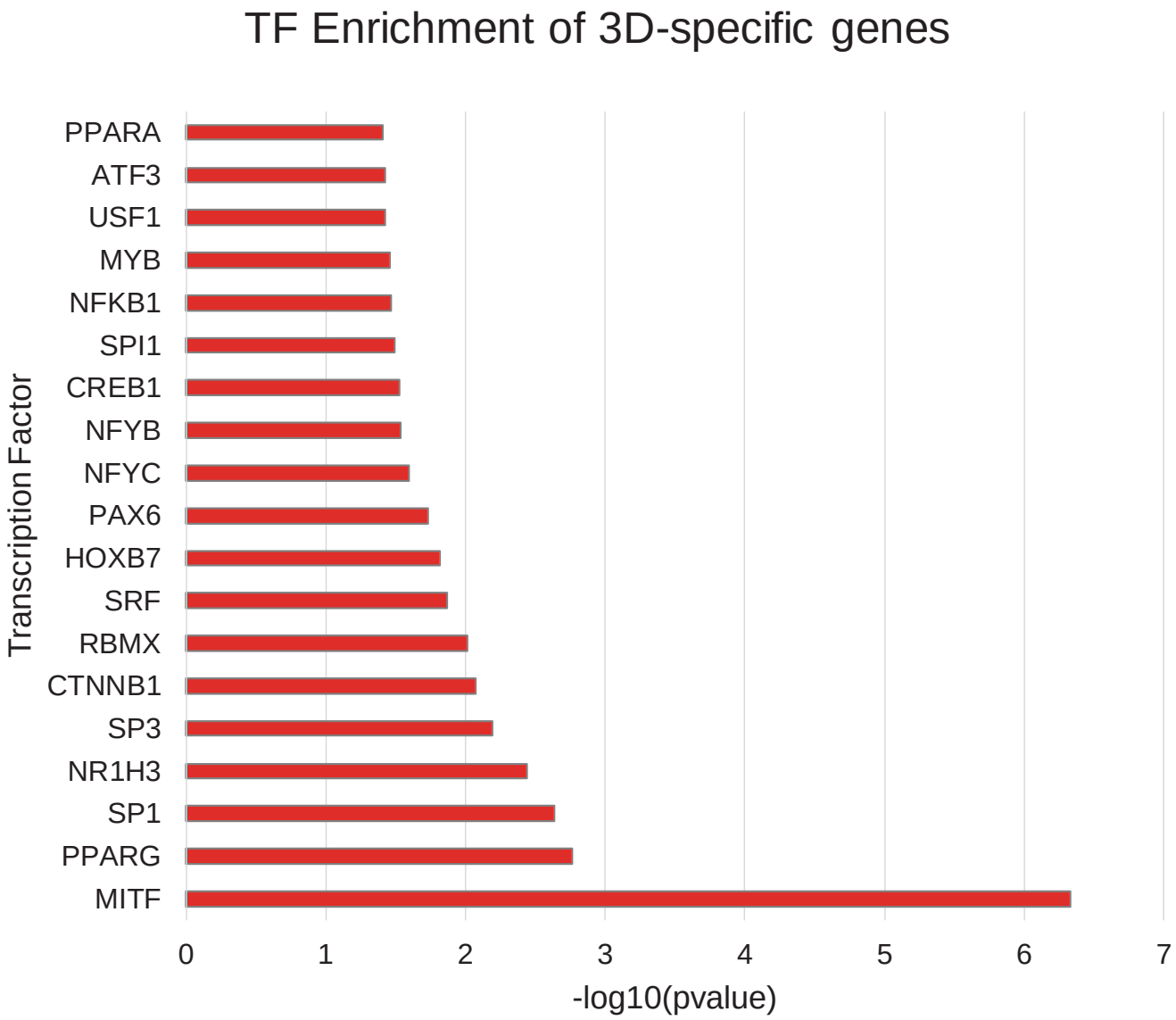

Online Figure IV. Predicted transcriptional regulators of 3D specific genes. Genes upregulated in 3D cardiac fibroblasts were assayed for enrichment of upstream transcriptional factors using TRRUSTv2. Significantly represented transcriptional components are plotted with corresponding p value enrichment among 3D genes.

3D down-regulated pathways

MODULE	FDR	GENE	LOCUS	VALUE	Description
GO:0006281	0.00%	Pif1	Pif1	28.39	DNA repair
GO:0006281	0.00%	Exo1	Exo1	17.72	DNA repair
GO:0006281	0.00%	Neil3	Neil3	15.45	DNA repair
GO:0006281	0.00%	Clspn	Clspn	14.42	DNA repair
GO:0006281	0.00%	Polq	Polq	13.91	DNA repair
GO:0007059	0.00%	Ska1	Ska1	31.16	chromosome segregation
GO:0007059	0.00%	Kif2c	Kif2c	27.23	chromosome segregation
GO:0007059	0.00%	Cenpf	Cenpf	26.66	chromosome segregation
GO:0007059	0.00%	Nek2	Nek2	22.36	chromosome segregation
GO:0007059	0.00%	Cenpe	Cenpe	19.4	chromosome segregation
GO:0000776	0.00%	Ska1	Ska1	31.16	kinetochore
GO:0000776	0.00%	Kif2c	Kif2c	27.23	kinetochore
GO:0000776	0.00%	Cenpf	Cenpf	26.66	kinetochore
GO:0000776	0.00%	Nek2	Nek2	22.36	kinetochore
GO:0000776	0.00%	Plk1	Plk1	20.1	kinetochore
GO:0006260	0.00%	Pif1	Pif1	28.39	DNA replication
GO:0006260	0.00%	Dscc1	Dscc1	17.22	DNA replication
GO:0006260	0.00%	Rrm2	Rrm2	14.56	DNA replication
GO:0006260	0.00%	Polq	Polq	13.91	DNA replication
GO:0006260	0.00%	Ticrr	Ticrr	12.63	DNA replication
GO:0005694	0.00%	Ska1	Ska1	31.16	chromosome
GO:0005694	0.00%	Kif2c	Kif2c	27.23	chromosome
GO:0005694	0.00%	Kif4	Kif4	24.66	chromosome
GO:0005694	0.00%	Nek2	Nek2	22.36	chromosome
GO:0005694	0.00%	Plk1	Plk1	20.1	chromosome
GO:0051301	0.00%	Anln	Anln	36.4	cell division
GO:0051301	0.00%	Ska1	Ska1	31.16	cell division
GO:0051301	0.00%	Kif2c	Kif2c	27.23	cell division
GO:0051301	0.00%	Aspm	Aspm	27.05	cell division
GO:0051301	0.00%	Cdc20	Cdc20	26.59	cell division

3D upregulated pathways

MODULE	FDR	GENE	LOCUS	VALUE	Description
GO:0009986	2.88%	Adamts15	Adamts15	173.38	cell surface
GO:0009986	2.88%	Cd36	Cd36	19.93	cell surface
GO:0009986	2.88%	Ciita	Ciita	8.01	cell surface
GO:0009986	2.88%	Apoe	Apoe	6.74	cell surface
GO:0009986	2.88%	Adgrv1	Adgrv1	6.71	cell surface
GO:0007166	2.48%	Agt	Agt	44.71	cell surface receptor signaling pathway
GO:0007166	2.48%	Cd36	Cd36	19.93	cell surface receptor signaling pathway
GO:0007166	2.48%	Adgrf4	Adgrf4	9.34	cell surface receptor signaling pathway
GO:0007166	2.48%	Adgrg1	Adgrg1	9.16	cell surface receptor signaling pathway
GO:0007166	2.48%	Cd22	Cd22	7.5	cell surface receptor signaling pathway

GO:0004950	2.19%	Ccr1	Ccr1	5.68	chemokine receptor activity
GO:0004950	2.19%	Ccr3	Ccr3	4.67	chemokine receptor activity
GO:0004950	2.19%	Ccr5	Ccr5	4.64	chemokine receptor activity
GO:0004950	2.19%	Ackr2	Ackr2	4.34	chemokine receptor activity
GO:0004950	2.19%	Ccrl2	Ccrl2	3.66	chemokine receptor activity
GO:0004930	1.42%	Adra1a	Adra1a	18.01	G-protein coupled receptor activity
GO:0004930	1.42%	Ackr1	Ackr1	13.01	G-protein coupled receptor activity
GO:0004930	1.42%	Adgrf4	Adgrf4	9.34	G-protein coupled receptor activity
GO:0004930	1.42%	Adgrg1	Adgrg1	9.16	G-protein coupled receptor activity
GO:0004930	1.42%	Adgrv1	Adgrv1	6.71	G-protein coupled receptor activity
GO:0070098	1.36%	Ccl6	Ccl6	30.3	chemokine-mediated signaling pathway
GO:0070098	1.36%	Ccl8	Ccl8	14.23	chemokine-mediated signaling pathway
GO:0070098	1.36%	Ackr1	Ackr1	13.01	chemokine-mediated signaling pathway
GO:0070098	1.36%	Ccl19	Ccl19	6.62	chemokine-mediated signaling pathway
GO:0070098	1.36%	Ccr1	Ccr1	5.68	chemokine-mediated signaling pathway
GO:0002376	1.11%	C2	C2	8.87	immune system process
GO:0002376	1.11%	Cd7	Cd7	7.01	immune system process
GO:0002376	1.11%	Cd24a	Cd24a	6.4	immune system process
GO:0002376	1.11%	Cd1d1	Cd1d1	6.23	immune system process
GO:0002376	1.11%	Clec4d	Clec4d	5.63	immune system process
GO:0048020	0.49%	Ccl6	Ccl6	30.3	CCR chemokine receptor binding
GO:0048020	0.49%	Ccl8	Ccl8	14.23	CCR chemokine receptor binding
GO:0048020	0.49%	Ccl19	Ccl19	6.62	CCR chemokine receptor binding
GO:0048020	0.49%	Ccl3	Ccl3	5.46	CCR chemokine receptor binding
GO:0048020	0.49%	Ccl9	Ccl9	4.88	CCR chemokine receptor binding
GO:0005615	0.35%	Adamts15	Adamts15	173.38	extracellular space
GO:0005615	0.35%	Ahsg	Ahsg	143.77	extracellular space
GO:0005615	0.35%	Cilp	Cilp	101.07	extracellular space
GO:0005615	0.35%	Agt	Agt	44.71	extracellular space
GO:0005615	0.35%	Ccl6	Ccl6	30.3	extracellular space
GO:0006955	0.35%	Ccl6	Ccl6	30.3	immune response
GO:0006955	0.35%	Cd36	Cd36	19.93	immune response
GO:0006955	0.35%	Ccl8	Ccl8	14.23	immune response
GO:0006955	0.35%	Ccr1	Ccr1	5.68	immune response
GO:0006955	0.35%	Ccl3	Ccl3	5.46	immune response
GO:0006935	0.34%	Ccl6	Ccl6	30.3	chemotaxis
GO:0006935	0.34%	Ccl8	Ccl8	14.23	chemotaxis
GO:0006935	0.34%	Ccr1	Ccr1	5.68	chemotaxis
GO:0006935	0.34%	Ccl3	Ccl3	5.46	chemotaxis
GO:0006935	0.34%	Ccl9	Ccl9	4.88	chemotaxis
GO:0005576	0.03%	Adamts15	Adamts15	173.38	extracellular region
GO:0005576	0.03%	Ahsg	Ahsg	143.77	extracellular region
GO:0005576	0.03%	Cilp	Cilp	101.07	extracellular region
GO:0005576	0.03%	Angptl7	Angptl7	35.5	extracellular region
GO:0005576	0.03%	Ccl6	Ccl6	30.3	extracellular region
GO:0009897	0.01%	Cd36	Cd36	19.93	external side of plasma membrane
GO:0009897	0.01%	Anpep	Anpep	14.75	external side of plasma membrane

GO:0009897	0.01%	Abcg1	Abcg1	12.08	external side of plasma membrane
GO:0009897	0.01%	Cd22	Cd22	7.5	external side of plasma membrane
GO:0009897	0.01%	Ace	Ace	7.03	external side of plasma membrane

Online Table II. Gene Ontology (GO) enrichment of differentially expressed genes in 3D/2D fibroblast states using marker set enrichment analysis. Genes weighted by differential expression in 3D vs 2D conditions were used for pathway enrichment. The top 5 genes in each module (GO Term) are shown, as well as enrichment parameters used for marker set enrichment analysis.

Cardiac Traits	PC1 bicor	PC1 pvalue	PC2 bicor	PC2 pvalue
LVID at end diastole	0.307153722	0.003061476	0.323570986	0.00175629
LVID at end systole	0.335373707	0.001155294	0.31977809	0.00200237
total heart mass	0.401094007	8.15E-05	0.382985671	0.00017906
Heart rate	-0.096279289	0.363951754	0.012565032	0.90590092
left atrium mass	-0.207355374	0.04858779	-0.194756892	0.06432276
left atrium mass/body weight	0.234401802	0.02532589	-0.126156765	0.23342204
Mitral inflow E to A velocity ratio	0.206913009	0.049080681	-0.181414515	0.08525588
Mitral inflow E velocity	0.142027866	0.179288492	0.027156442	0.79832003
right atrium mass	0.141874927	0.17976205	-0.213481134	0.0421724
right ventricle mass	0.248416495	0.017580812	-0.136692434	0.19635339
PW thickening	-0.141602933	0.180606502	-0.027406706	0.79650139
IVS at end diastole	0.118263577	0.264212253	0.047024272	0.65803569
Fractional shortening	-0.117997784	0.265294858	0.069023215	0.51561902
Ejection fraction	-0.116547941	0.271253069	0.069464983	0.51292866
IVS to PW ratio at end systole	0.110277742	0.298052867	0.140994675	0.18250542
Mitral inflow A to E velocity ratio	-0.105389119	0.320114602	0.097216285	0.35927989
Velocity of circumferential shorteni	-0.092840053	0.381417667	0.020914209	0.84400568
Aortic valve ejection time	-0.041190146	0.698266367	-0.006581397	0.95063029
right atrium mass/body weight	-0.031229221	0.768863947	-0.162622492	0.12352472
Relative wall thickness at end diasto	0.021042494	0.843061023	0.004800975	0.96397537
Non-Cardiac Traits	**PC1 bicor**	**PC1 pvalue**	**PC2 bicor**	**PC2 pvalue**
glucose	0.071762413	0.49905418	0.079651552	0.45294327
liver mass	0.419959472	3.41E-05	-0.204154599	0.05224801
body weight	0.356474817	0.000523921	-0.217214	0.03862046
adrenal mass/body weight	0.017261024	0.870994403	-0.068477455	0.5189526
lung mass	0.314333443	0.002410094	-0.191032842	0.06969477
lung mass/body weight	0.028022775	0.792029117	-0.148271069	0.16072745
free fatty acids	0.261513514	0.012282178	-0.349471421	0.00068532
unesterified cholesterol	-0.001138736	0.991452678	-0.215058364	0.0406398
total cholesterol	0.058346891	0.582752968	-0.338164028	0.00104384
HDL	0.204694279	0.051615441	-0.340203757	0.00096866
trigycerides	0.197385148	0.060737614	-0.103279085	0.32995308
adrenal mass	0.159128625	0.131907152	-0.101031122	0.3406441
liver mass/body weight	0.237248848	0.023552203	-0.168058428	0.1113036

Online Table III. Traits measured in the HMDP following infusion of isoproterenol and their correlation with principal components based on genes upregulated in 3D fibroblasts. Individual cardiac and non-cardiac traits were plotted against the strain position on each component axis (as illustrated in Figure 3C-L). From these correlations, bicorrelation coefficients and corresponding p-values were calculated for each PC x trait relationship. Traits illustrated in Figure 3 are highlighted with a grey background.

Gene	adjusted pvalue
Adamts15	6.26E-07
Ahsg	2.05E-21
Cilp	4.22E-06
Wfdc3	1.96E-25
Ptgds	4.14E-13
Ctrb1	5.63E-05
Fndc5	2.46E-07
Agt	2.79E-16
Angptl7	1.16E-07
Dkk3	5.87E-27
Fam180a	4.03E-12
Igfbp5	1.62E-28
Mmp11	2.03E-228
Htra3	1.39E-07
Penk	0.008313927
Emid1	0.005125138
Fbln7	8.73E-23
Plin4	1.19E-06
Ccl8	0.000140485
Mmp2	3.15E-26
Mamdc2	5.10E-38
Sparcl1	1.66E-05
Fam198a	2.13E-05
Tgfbi	2.13E-32
Fgl2	8.79E-09
Il1rn	0.009482538
Epor	0.001064303
Pik3ip1	4.01E-10
Enpp3	1.77E-25
Enpp2	7.36E-05
C2	0.0008716
Col9a2	0.001275955
Lpl	0.002443402
Mfap2	9.54E-11
Fbln1	0.000326378
Pamr1	0.000697679
Lgi4	1.64E-09
Smoc2	3.10E-05
Sepp1	5.53E-19
Adamtsl2	2.79E-11
C1ql1	0.000609573
Sned1	1.21E-05
Apoe	0.001412247
Iglon5	4.34E-11
Vash1	0.005782713
Clu	0.00605853

Dpt	0.008989791
Pla2g2e	0.000201816
Serpine2	4.13E-10
Dpp7	7.48E-19
Ssc5d	1.21E-06
Cpz	0.002400706
Islr	6.52E-06
Psap	0.008066424
Matn4	2.40E-09
Creg1	0.002226995
Ephb6	1.32E-08
Matn2	1.81E-05
Fam19a5	0.000596104
Sorl1	0.003374037
Slc17a5	0.000125364
Ctsl	3.23E-05
Hsd17b11	4.15E-18
Sord	2.79E-06
Ifi30	0.009015165
Sdc1	0.002285504
Tcn2	0.001758118
Gnptg	0.00861747
Grn	0.004461313
Txndc16	6.76E-07
Scpep1	3.31E-17
Mmp19	0.002352839
Glb1l	4.94E-05

Online Table IV. Genes upregulated in 3D cardiac fibroblasts filtered for secreted factors. Genes upregulated in the 3D cardiac fibroblast state were filtered for secreted factors by overlaying the gene symbol of 3D specific transcripts with deposited data of known secreted factors within the Universal Protein Resource (UniProt) using the following accessions: location:"Secreted [SL-0243]" type:component AND organism:"Mus musculus (Mouse) [10090]. The p values listed were generated from differential expression analysis of 3D vs 2D transcripts using a 10% FDR.

*** Long In Vivo Checklist**

Circulation Research - Preclinical Animal Testing: A detailed checklist has been developed as a prerequisite for every publication involving preclinical studies in animal models. ***Checklist items must be clearly presented in the manuscript, and if an item is not adhered to, an explanation should be provided.*** *If this information (checklist items and/or explanations) cannot be included in the main manuscript because of space limitations, please include it in an online supplement. If the manuscript is accepted, this checklist will be published as an online supplement. See the explanatory editorial for further information.*

This study involves use of animal models:

Yes

Study Design

The experimental group(s) have been clearly defined in the article, including number of animals in each experimental arm of the study.	Yes
An overall study timeline is provided.	Yes
The protocol was prospectively written	Yes
The primary and secondary endpoints are specified	Yes
For primary endpoints, a description is provided as to how the type I error multiplicity issue was addressed (e.g., correction for multiple comparisons was or was not used and why). (Note: correction for multiple comparisons is not necessary if the study was exploratory or hypothesis-generating in nature).	Yes
A description of the control group is provided including whether it matched the treated groups.	Yes

Inclusion and Exclusion criteria

Inclusion and exclusion criteria for enrollment into the study were defined and are reported in the manuscript.	Yes
These criteria were set *a priori* (before commencing the study).	Yes

Randomization

Animals were randomly assigned to the experimental groups. If random assignment was not used, adequate explanation has been provided.	Yes
Type and methods of randomization have been described.	Yes
Allocation concealment was used.	Yes
Methods used for allocation concealment have been reported.	Yes

Blinding

Blinding procedures with regard to masking of group/treatment assignment from the experimenter were used and are described. The rationale for nonblinding of the experimenter has been provided, if such was not performed.	Yes
Blinding procedures with regard to masking of group assignment during outcome assessment were used and are described.	Yes
If blinding was not performed, the rationale for nonblinding of the person(s) analyzing outcome has been provided.	Yes

Sample size and power calculations

Formal sample size and power calculations were conducted before commencing the study based on *a priori* determined outcome(s) and treatment effect(s), and the data are reported.	Yes
If formal sample size and power calculation was not conducted, a rationale has been provided.	Yes

Data Reporting

Baseline characteristics (species, sex, age, strain, chow, bedding, and source) of animals are reported.	Yes
The number of animals in each group that were randomized, tested, and excluded and that died is reported. If the experimentation involves repeated measurements, the number of animals assessed at each time point is provided is provided for all experimental groups.	Yes
Baseline data on assessed outcome(s) for all experimental groups are reported.	Yes
Details on important adverse events and death of animals during the course of the experiment are reported for all experimental groups.	Yes
Numeric data on outcomes are provided in the text or in a tabular format in the main article or as supplementary tables, in addition to the figures.	Yes
To the extent possible, data are reported as dot plots as opposed to bar graphs, especially for small sample size groups.	Yes
In the online Supplemental Material, methods are described in sufficient detail to enable full replication of the study.	Yes

Statistical methods

The statistical methods used for each data set are described.	Yes
For each statistical test, the effect size with its standard error and *P* value is presented. Authors are encouraged to provide 95% confidence intervals for important comparisons.	Yes
Central tendency and dispersion of the data are examined, particularly for small data sets.	Yes
Nonparametric tests are used for data that are not normally distributed.	Yes
Two-sided *P* values are used.	Yes
In studies that are not exploratory or hypothesis-generating in nature, corrections for multiple hypotheses testing and multiple comparisons are performed.	Yes
In "negative" studies or null findings, the probability of a type II error is reported.	Yes

Experimental details, ethics, and funding statements

Details on experimentation including formulation and dosage of therapeutic agent, site and route of administration, use of anesthesia and analgesia, temperature control during experimentation, and postprocedural monitoring are described.	Yes
Both male and female animals have been used. If not, the reason/justification is provided.	Yes
Statements on approval by ethics boards and ethical conduct of studies are provided.	Yes
Statements on funding and conflicts of interests are provided.	Yes

---

Date completed: 04/19/2018 15:56:25
User pid: 11913